Final Scientific/Technical Report

Chromium Tolerant, Highly Active and Stable Electrocatalytic Internal Surface Coating for Cathode of Commercial SOFCs

DE-FE0031665

Recipient: West Virginia University Research Corporation

August 21, 2018 to August 20, 2022

Principle Investigator: Xueyan Song, Ph.D.,
Professor,
George B. Berry Chair Professor of Engineering
Department of Mechanical and Aerospace Engineering,
West Virginia University
Tel: 304-293-3269,
Email: xueyan.song@mail.wvu.edu

DISCLAIMER

Abstract

This project is aimed to develop chromium (Cr) tolerant, highly active, and stable coating layers on the internal surfaces of the porous composite cathodes from inherently functional commercially available SOFCs. Such coating layers were developed using the additive manufacturing process of Atomic Layer Deposition (ALD), and have been applied on the cathode consisting of either an electronic conductor of $La_xSr_{1-x}Mn_yO_{3-\delta}$ (LSM) or mixed ionic and electronic conducting $La_xSr_{1-x}Co_yFe_{1-y}O_{3-\delta}$ (LSCF).

The PI's work has demonstrated that the internal surface of the cathode from the commercial cells can be further tailored using an ALD coating to enhance the cell performance dramatically. For instance, the ALD layer consisting of heterostructured nanocomposite of nano-Pt and nano-$(Mn_{0.8}Co_{0.2})_3O_4$ oxide on the internal surface of porous LSM/YSZ cathode from SOFCs, has resulted in the large reduction of the cell polarizations resistance by up to 53%, and the enormous increase of power density over 370%. For the cells with LSCF / Sm_2O_3 doped CeO_2 (SDC) cathode, the conformal layer of nano-composite consisting of superjacent CoO_x and subjacent minimum amount of Pt nano-grains has resulted in the power density enhancement of 126 % for the large-scale industry tubular cells at 750℃. Both the performance enhancement and nanostructure of the ALD layer were stable for over ~ 2000 h of continuous operation performed at the industry test station. Meanwhile, the ALD coating layer developed by PI's work is also inherently Cr-tolerant and could act as a physical barrier for preventing Cr diffusion into the cathode backbone so as to mitigate the Cr poisoning effect on the cathode. In this project, the impact of Cr on the performance of those ALD-coated commercial cells has been evaluated. Based on the evolution of the cell performance, the ALD coating layer chemistry and ALD coating layer thickness have been optimized to maximize the overall Cr tolerance, cell power density, and cell longevity.

Different ALD coatings have been applied onto the internal surface of LSM/YSZ and LSCF/SDC backbone respectively. The architecture/scaffold structures on the internal surface of different cathode, designed by this project, was catalogued and analyzed using High Resolution Transmission Electron Microscopy (HRTEM), and cell power/durability performance are assured

Abstract

via comprehensive electrochemical performance testing under industry operation relevant conditions. The impact of the electrochemical operation current density, the water humidity, the cell operation temperature, and cell operation duration on the Cr tolerance of ALD coated cells has been systematically investigated.

There are completely different nanostructure degradation mechanisms between LSM and LSCF cells induced by Cr contamination. For the LSCF/SDC baseline cell, with the Cr source, there is no apparent Sr surface segregation phase even for the baseline cell operated for 3000 h at 750 ºC. With the Cr source, there is a significant amorphous (SrCr)Ox phase accumulation in the original pore region. For the commercial baseline cells, Cr contaminants on the LSM electrode severely impacted the electrochemical performance and nanostructure degradation of the entire cell. Those degradations include: (1). Peak power density loss of 64 % after 109 h of operation, with the dramatic increase in $R_{p.}$ (2). The cracking at the LSM/SSZ interface, LSM grains. The SSZ remains intact but with (CrMn)Ox deposited. By contrast, ALD coating (MnCo)Ox/Pt dramatically improves the Cr resistance, as follows: (1). ALD-coated cell with a power density is 280-380% of the baseline cell, depending on the ALD layer thickness. (2). For a cell with a 20 nm thick ALD layer, there is a large performance enhancement (> 200% power density) induced by ALD coating of Cr-tolerant $Mn_{0.8}Co_{0.2}O_x$. (3). For a cell with a 20 nm thick ALD layer, after 168 h at 750ºC the power density of the ALD-coated cell is ~ 600 % better than the baseline cell upon operation with Cr contamination for 109 h.

The ALD coating on the internal surface of cathode developed by this project integrated multi-functions. Those multi-functions include (1). Dramatically improving the cell power density for the commercial cells; (2). Dramatically improving contamination resistance of the cathode, being an excellent protection coating layer, and sealing off Cr contamination. (3). Dramatically increasing the cell longevity by potentially preventing the microstructure evolution and grain coarsening of the cathode. Overall, this project will provide a simple solution to simultaneously enhancing power density, and increasing reliability, robustness and endurance of

Abstract

commercial SOFCs. This project directly supports the research and development of large-scale fuel cell stacks used in industry. Most importantly, the proposed ALD infiltration technology uses computer controlled automatic processing, and is simple, time efficient, cost-effective and scale-up ready for annual production.

Table of Contents

Chromium Tolerant, Highly Active and Stable Electrocatalytic Internal Surface Coating for Cathode of Commercial SOFCs

2 Executive Summary

This project is aimed to develop a chromium (Cr) tolerant, highly active, and stable coating layer on the internal surfaces of the porous composite cathode of commercially available SOFCs. Such a coating layer was developed using the additive manufacturing process of Atomic Layer Deposition (ALD) and has been applied on the cathode consisting of either an electronic conductor of $La_xSr_{1-x}Mn_yO_{3-\delta}$ (LSM) or mixed ionic and electronic conducting $La_xSr_{1-x}Co_yFe_{1-y}O_{3-\delta}$ (LSCF).

The PI's work has demonstrated that the internal surface of cathode from the commercial cells, can be further tailored using ALD coating to dramatically enhance the cell performance. For instance, an ALD layer consisting of a heterostructured nano composite of nano-Pt and nano-$(Mn_{0.8}Co_{0.2})_3O_4$ oxide on the internal surface of porous LSM/YSZ cathode from SOFCs, has resulted in the large reduction of the cell polarizations resistance by up to 53%, and enormous increase of power density of over 370%. For the cells with an LSCF / Sm_2O_3 doped CeO_2 (SDC) cathode, the conformal layer of nano-composite consisting of superjacent CoO_x and subjacent minimum amount of Pt nano-grains has resulted in the power density enhancement by 126% for the large scale industry tubular cells at 750℃, and both the performance enhancement and nanostructure of the ALD layer are stable over ~ 2000 h continuous operation performed at an industry test station. In the meanwhile, those ALD coating layers developed by PI's work are also inherently Cr-tolerant, and could act as physical barriers for preventing Cr diffusion into the cathode backbone, so as to mitigate the Cr poisoning effect on the cathode. In this project, the impact of Cr on the performance of those ALD coated commercial cells has been evaluated. Based on evolution of the cell performance, the ALD coating layer chemistry and ALD coating layer thickness has been optimized to maximize the overall Cr tolerance, cell power density and cell longevity.

Different ALD coatings have been applied onto the internal surface of LSM/YSZ and

LSCF/SDC backbone, respectively. The architecture/scaffold structures on the internal surface of different cathode, designed by this project, was catalogued and analyzed using High Resolution Transmission Electron Microscopy (HRTEM), and the cell power/durability performance is assured via comprehensive electrochemical performance testing at the industry operation relevant conditions. The impact of the electrochemical operation current density, the water humidity, the cell operation temperature, and cell operation duration on the Cr tolerance of ALD coated cells has been systematically investigated.

There are completely different nanostructure degradation mechanisms between LSM and LSCF cells induced by Cr contamination. For the LSCF/SDC baseline cell, with the Cr source, there is no apparent Sr surface segregation phase even for the baseline cell operated for 3000 h at 750 ºC. With the Cr source, there is significant amorphous (SrCr)Ox phase accumulated in the original pore region.

For the commercial baseline cells, Cr contaminants on the LSM electrode severely impacted the entire cell's electrochemical performance and nanostructure degradation. Those degradations include: (1). Peak power density loss of 64 % after 109 h of operation with dramatic increase in R_p.(2). Cracking at LSM/SSZ interface, LSM grains. SSZ remains intact but with (CrMn)Ox deposits. By contrast, the ALD coating (MnCo)Ox/Pt dramatically improves the Cr resistance, as follows: (1). ALD-coated cell with a power density is 280-380 % of the baseline cell, depending on the ALD layer thickness. (2). For a cell with a 20 nm thick ALD layer, there is a large performance enhancement (> 200 % power density) induced by an ALD coating of Cr-tolerant $Mn_{0.8}Co_{0.2}O_x$. (3). For a cell with a 20 nm thick ALD layer, after 168 h at 750 ºC the power density of the ALD-coated cell is ~ 600% better than the baseline cell operating with Cr contamination for 109 h.

The ALD coating on the internal surface of cathode developed by this project integrated multi-functions. Those multi-functions include (1). Dramatically improving the cell power density for the commercial cells; (2). Dramatically improving contamination resistance of the cathode, for being an excellent protection coating layer sealing off Cr contamination. (3). Dramatically

increasing the cell longevity by potentially preventing the microstructure evolution and grain coarsening of the cathode.

Overall, this project will provide a simple solution to simultaneously enhancing power density, and increasing reliability, robustness and endurance of commercial SOFCs. This project directly supports the research and development of large-scale fuel cell stacks in industry. Most importantly, the proposed ALD infiltration technology is computer-controlled automatic processing, and is simple, time efficient, cost-effective and scale-up ready for annual production.

3 Comparison of the actual accomplishment with the goals and objectives

Proposed goals and objectives: Our ***target material*** systems are commercial ***LSM/YSZ*** and ***LSCF/SDC*** composite electrodes, respectively, and emphasis will be towards applications at temperatures of 650-800ºC. The research objectives are to develop the Cr-tolerant of LSM/YSZ and LSCF/SDC cathode cathodes, through the ALD coating of inherently functional commercial cells. The ALD coating on the internal surface of cathode developed by this project will integrate **multi-functions.** Those multi-functions include: **(1)**. Dramatically **improving contamination resistance** being an excellent protection coating layer **sealing off the chromium contamination**. (2). Dramatically **improving the cell performance by a factor over 1.5** for the commercial cells; (3). Dramatically **increasing the cell longevity** being a **stable nanostructure,** at the internal surface of porous cathode, upon high temperature cell operation**. With optimized design of the cathode surface nanostructure using ALD, the technical achievement on the commercial cells, in the environments of presence of Cr, is expected to be 50 % greater in power density** throughout the entire SOFC operation temperature range of 650-800 ºC. Overall, this project will provide **a simple solution** to **simultaneously** enhancing power density, and increasing reliability, robustness and endurance of commercial SOFCs, over the entire operational temperature range of 650-800 ºC.

Actual Accomplishment: In terms of the chemistry of the ALD layer, this project has employed a commercially relevant electrolyte, electrocatalyst, and noble metal materials set. Such materials are fully compatible with commercial fuel cells, and this project has developed a special nanostructure on the surface of commercial composite cathodes. With the support of this award, the following has been achieved:

Accomplishment -1: For the first time in the field of SOFC, the detailed nanostructure evolution of the LSM and LSCF baseline cells induced by Cr contamination upon electrochemical operation was systematically studied. There are completely different nanostructure degradation mechanisms between LSM and LSCF cells induced by Cr contamination. The impact of the electrochemical operation current density, the cell operation temperature, and cell operation duration on the Cr tolerance of ALD coated cells has been systematically investigated.

Accomplishment -2: It has been revealed through this project that for the LSCF/SDC baseline cell, with the Cr source, there is no apparent Sr surface segregation phase even for the baseline cell operated for 3000 h at 750 ºC. With the Cr source, there is significant amorphous (SrCr)Ox phase accumulated in the original pore region.

Accomplishment -3: For the commercial baseline cells, Cr contaminants on the LSM electrode severely impacted the electrochemical performance and nanostructure degradation of the entire cell. Those degradation include: (1). Peak power density loss of 64% after 109 h operation. Dramatic increase in R_p (2). Cracking at LSM/SSZ interface, LSM grains. SSZ remains intact, but with (CrMn)Ox deposited. By contrast, an ALD coating (MnCo)Ox/Pt dramatically improves the Cr resistance, as follows: (1). ALD coated cell is with power density 280-380 % of the baseline cell depending on the ALD layer thickness. (2). For a cell with a 20 nm thick ALD layer, there is a large performance enhancement (> 200 % power density) induced by the ALD coating of Cr-tolerant $Mn_{0.8}Co_{0.2}O_x$. (3). For a cell with 20 nm thick ALD layer, after 168 h at 750□C power density of ALD-coated cell is ~ 600 % of that baseline cell upon operation with Cr contamination for 109 h.

The ALD coating on the internal surface of the cathode developed by this project integrated multi-functions. Those multi-functions include: (1). Dramatically improving the cell power density for the commercial cells; (2). Dramatically improving contamination resistance of the cathode, for being an excellent protection coating layer sealing off Cr contamination. (3). Dramatically increasing the cell longevity by potentially preventing the microstructure evolution and grain coarsening of the cathode.

Overall, this project will provide a simple solution to simultaneously enhancing power density and increasing the reliability, robustness, and endurance of commercial SOFCs. This project directly supports the research and development of large-scale fuel cell stacks by industry. Most importantly, the proposed ALD infiltration technology is computer-controlled automatic processing and is simple, time efficient, cost-effective, and scale-up ready for annual production. For the first time in the field of SOFC, our study demonstrates an effective approach for solving

multiple problems for successfully suppressing the Sr surface segregation of mixed conductors, preventing Cr contamination, and simultaneously increasing the conductivity. The high-density surface and intergranular grain boundaries of the strained ALD layer provide an enormous surface area and interface area for facilitating multiple mass transport and catalytic reactions. It opens new research directions in terms of the fundamental design of the grain boundaries and strained critical interface for electrochemical reactions at elevated temperatures.

The approaches utilized in this project could enable increased electrical power of SOFCs at low operating temperature. The success of this project demonstrated the commercial scalability of the ALD processing with minimal impact to the cost structure of the cells and the stacks.

4 Performance and Nanostructure Degradation of LSM Cathode Induced By Cr contamination

4.1 Introduction

4.1.1 Chromium poisoning of the cathode, associated interconnect coating, and its technical challenges

Individual SOFC cells need to be connected electrically, in series, to form stacks in order to generate the desired power output with high voltage, using the interconnect. Thus, the interconnect materials should have high electrical conductivity, negligible ionic conductivity and be chemically and structurally stable under both air and fuel environment. There are basically two types of interconnect materials commonly used in SOFCs which are doped LaCrO3-based ceramic materials and metallic materials. Compared to the ceramic interconnect materials, metallic materials have high electronic and thermal conductivity, negligible ionic conductivity, good machinability and low cost. However, metal alloys of high temperature oxidation resistance used as interconnect in SOFCs generally contain Cr as an alloying element to form a protective chromium oxide scale (Cr2O3). At high temperatures volatile Cr species such as CrO3 and Cr(OH)2O2 are generated over the oxide scale. [1] Volatilization of Cr species strongly depends on the oxygen partial pressure and the water content. [2,3,4] In the cathode end, at high temperatures volatile Cr species such as CrO3 and Cr(OH)2O2 are generated over the oxide scale in oxidizing atmospheres. Such volatile Cr species subsequently poison and react with the cathodes such as LSM and LSCF, causing a rapid degradation of the cell performance.

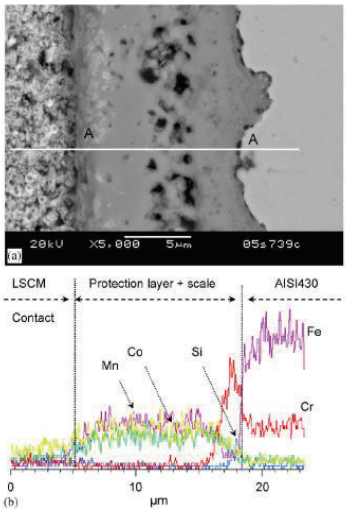

Fig. 1 (MnCo)Ox interconnect coating structure on LSM.

The chromium volatility can be suppressed by modification of the metallic interconnect materials. For example, the interconnect can be surface-modified via application of coating of conductive oxide(s). The coating layer is intended to serve as a barrier to both chromium cation

outward and oxygen anion inward diffusion. For a ferritic stainless-steel interconnect, the (Co,Mn)3O4 spinel is usually applied as the coating layer. [5] Upon oxidation, a thin (Cr,Mn)3O4 layer is formed at the interface between steel substrate and the (Co,Mn)3O4 coating layer, and effectively prevents Cr migration from the steel substrates to the surface, as shown in Fig. 1. [5] Thus, the electric conducting (Co,Mn)3O4 spinel coating effectively acts as a Cr transport barrier to retard rapid Cr2O3-scale growth and Cr evaporation.

For the Mn–Co spinel interconnect coating, selection of appropriate deposition technique is critically important, the consideration of deposition techniques shall not only be focused on cost, but also on their workability on interconnects with complicated gas flow channels. Most importantly, the microstructure and surface quality of coating layer is often found to impact the fuel cell stack performance.

The interaction between metallic interconnect and cathodes of SOFCs, and the associated interconnect coating have been extensively investigated in the last 10-15 years. However, despite the intense effort of the past decade, for the coating layer fabricated using different techniques, there are still occurrence of spallation between coating/metal interfaces and increasing oxidation rate over time. Hence, long-term stability of interconnect materials must be improved. [6]

4.1.2 Mechanisms of Cr poisoning SOFC cathode

Complementary to the interconnect coating, one of the alternative and effective techniques to mitigate Cr-poisoning, is the development of cathode materials not only with high electrochemical activity and good stability, but also with excellent tolerance to impurities, particularly volatile Cr species from the chromia-forming metallic interconnect.

Development of Cr-resistant cathode requires the understanding of Cr-poisoning mechanisms. For the SOFC cathode, Cr deposition is controlled by the chemical reduction of high valence Cr species and subsequent nucleation and reaction processes of Cr species on the cathode. It has been well recognized that the mechanism and kinetics of Cr poisoning changes as the cell operation polarization changes. Furthermore, the Cr poisoning mechanisms differ dramatically from the LSM/YSZ cathode to the LSCF/SDC cathodes as briefed in the following.

For the cell with a LSM/YSZ composite cathode, both $(CrMn)_3O_4$ spinel and Cr_2O_3 phases were identified as a Cr poisoning product for LSM/YSZ cathode. In the meanwhile, the current load and cell operation has a dramatic impact on the Cr-poisoning of LSM/YSZ cells. A uniform chromium distribution on LSM/YSZ surface was observed under OCV conditions, while chromium deposition mainly occurred near the triple phase boundaries (TPBs) region under a current load [7,8]. Formation of Cr-containing phases resulted in increase in the activation overpotential, although a slight increase in the ohmic resistance was also observed. These findings indicate that the main factor causing degradation by chromium is not the chemical reaction between LSM and chromium but the electrochemical reaction of chromium oxide at the TPBs. The deposited various chromium oxide may block the diffusion pathways of reactant gas species to the electrode reaction sites, i.e, TPBs, and decrease the local exchange current density. Most importantly, the formation of the $(CrMn)_3O_4$ with the Mn coming from LSM will result in the Mn deficient LSM composition that deteriorates the LSM backbone performance.

4.1.3 ALD coating & its technical challenges for infiltrating Cr-tolerant layer on SOFC cathode

Enhanced Cr tolerance through solution-based infiltration: The mechanism of Cr deposition process described above implies that an electrode surface coating layer, which is **inert to Cr inward diffusion** to cathode could act **as barrier layer to prevent the direct reaction between the Cr with electrode**, and enhance the Cr tolerance. For example, for the LSCF/SDC composite electrode, there is evidence that solution-based cathode infiltration[9,10,11,12,13,14,15] of chromium inert phases, such as ionic-conducting $Ce_{0.9}Gd_{0.1}O_{2-d}$ (GDC), could mitigate the Cr poisoning [16]. The impregnated GDC nano-particles may act as a buffer layer to prevent the direct contact between LSCF and chromium species, improving the cathode tolerance towards Cr deposition.

From the **structure** point of view, the Cr-tolerant surface coating layer on the SOFC cathode needs to be: ***Deeply penetrating into the active layer*** of the cathode; ***Uniform and conformal*** on the internal surface of the cathode active layer that possess complex three-dimensional

topographies with high aspect ratio; ***Intimate adhesion and bonding*** to the cathode surface at atomic scale without spallation; Magnetron sputtering, sol-gel dip-coating, and electrodeposition techniques are used for applying protective coating on ferritic stainless-steel interconnects. Those deposition techniques involve **physical vapor deposition or liquid solutions**. None of those interconnect coatings will be ideal for infiltrating the cathode surface since they have the limitation of not deeply penetrating into the cathode active layer or not providing the conformal coating on cathode surface.

4.2 Experimental section

Commercially available, anode-supported solid oxide button cells fabricated by CTG (Salt Lake City, UT) were employed for all the experiments described in this paper. MSRI cells are composed of five layers as follows, starting from the anode: a ~700 μm thick Ni/YSZ cermet layer which supports the cell structure; a ~10 μm thick Ni/YSZ active layer; a ~10 μm thick YSZ electrolyte; a thin (2-3 μm), dense Sm_2O_3-doped CeO_2 (SDC) barrier layer, a ~10 μm thick LSM/YSZ or LSM/SSZ active layer; and a 50 μm thick, pure LSM current collecting layer. The cell active area (limited by the cathode) is 2 cm^2. The exposure area of the anode to fuel is about 3.5 cm^2.

A set of experiments were carried out in a Cr-rich environment and a different set of samples were analyzed in a Cr-free environment to see the influence of Cr in the air electrodes of the cell. Inconel 600 mesh was used as Cr source to create a Cr-rich environment in the air electrode side. The active area of the cells is limited by the cathode, as such both the power density and current density are calculated considering this area even if the anode exposure to fuel is larger in area than the active area of the cathode. In our test, the LSM/SSZ button cell as-fabricated by CTG was subject to operation on a single cell test station at 750 C under a Cr source for ~200 h. A multilayer-mesh stack was used as the inter-connect. The mesh stack includes 3 layers of Pt mesh and two layers of Inconel 600 mesh. The chemical composition of Inconel 600 used in this study is Al ~0.2, Co 0.03, Cr 16.05, Fe 8.6, Mn 0.45, NI 73.7 Ti 0.21 and other 0.76 (all in wt %).

All cell tests were performed on a test stand. The platinum mesh was used for anode and

cathode lead connections. The fuel and air stream flow rates were controlled separately using mass flow controllers. During the operation, a 400 mL/min air flow rate and a 400 mL/min fuel flow rate were used. Before any electrochemical measurements, both cells were current-treated for approximately ~15 h under a small current density of 0.1 A/cm^2 to ensure they were activated. After that, the samples were loaded at a constant current of 0.3 A/cm^2 for desired periods. The cell performance was examined using a TrueData-Load Modular Electronic DC Load, which guarantees voltage and current accuracies of 0.03 % FS of the range selected +/-0.05 % of the value. The cell impedance spectra were examined using a potentiostat/galvanostat (Solartron 1287A) equipped with a frequency response analyzer (Solartron 1260). Impedance measurements were carried out using a Solatron 1260 frequency response analyzer in a frequency range from 50 mHz to 100 KHz. The impedance spectra and resistance (Ωic resistance Rs and polarization resistance Rp) presented are those measured under a DC bias current of 0.3 A/cm^2. On a Nyquist plot, Rs is determined by the intercept at the higher frequency end, and Rp is determined by the distance between two intercepts.

After the electrochemical operation, the ALD coated cells were sectioned and subjected to nanostructural and crystallographic examination using high resolution (HR) Transmission Electron Microscopy (TEM). All the TEM examinations were conducted in the cathode active layer. TEM samples were prepared by mechanical polishing and ion milling in a liquid-nitrogen-cooled holder. Electron diffraction, diffraction contrast, and HRTEM imaging were performed using a JEM-2100 operated at 200 kV. Chemical analysis was carried out under TEM using energy dispersive X-ray Spectroscopy (EDS).

4.3 Impact of Cr Contamination on the Performance of Cathode and Entire Cell

Before operation, the cell was heated up to 750 ºC, reduced with 10 % H^2 and 33 % H^2 for ~ 6 h and then rest at open circuit voltage for ~ 26 h. After that, the cell was loaded with a current density of 0.3 A/cm^2 and operated for ~175 h as shown in Figure 2. The impedance data were taken periodically. Between 134 h and 144 h, we removed the current load and waited ~ 10 h for the recovery of the cell.

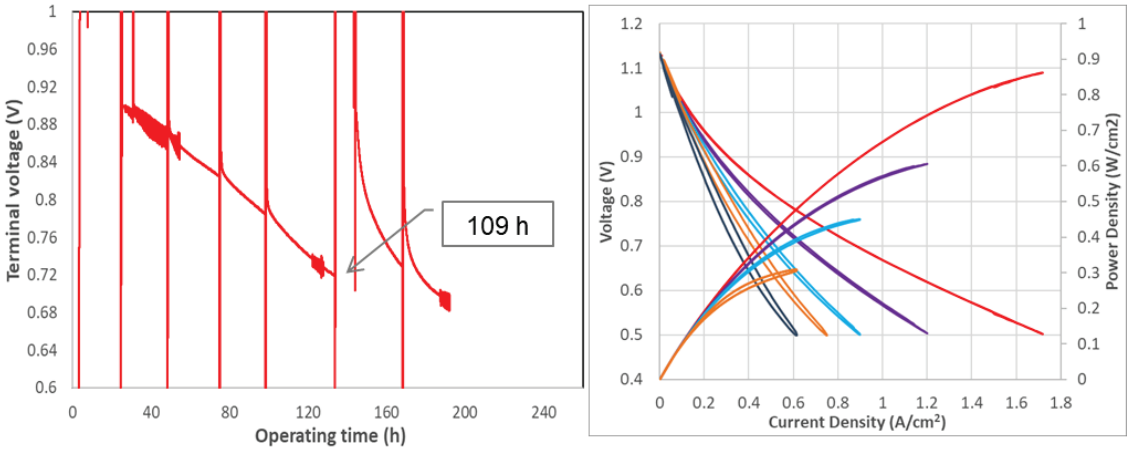

Operating time (h)	Peak power density (W/cm²)	Percentage degradation (%)
0	0.862	-
24	0.605	29.8 %
50	0.45	47.8 %
74	0.375	56.5 %
109	0.307	64.4 %

Figure 2 terminal voltage as a function of time for the CTG LSM/YSZ cell operated at 0.3 A/cm3 and 750 oC. P-i curves for the LSM baseline cell operated at 750 oC with Inconel 600.

As shown in Figure 3, the power is 0.308 W/cm^2 at 109 h and only 36 % of its initial power density. For the baseline cell, 100 h operation, the terminal voltage dropped ~ 190 mV. At 0.3 A/cm^2; the baseline cell exhibited degradation rate is 1.68 V per 1000 h.

Between 134 h and 144 h, the current load was removed. Once the current is re-loaded, the terminal voltage was back up to ~0.9 V (in Figure 3), and almost the same as the initial terminal voltage at 0.3 A/cm^2.

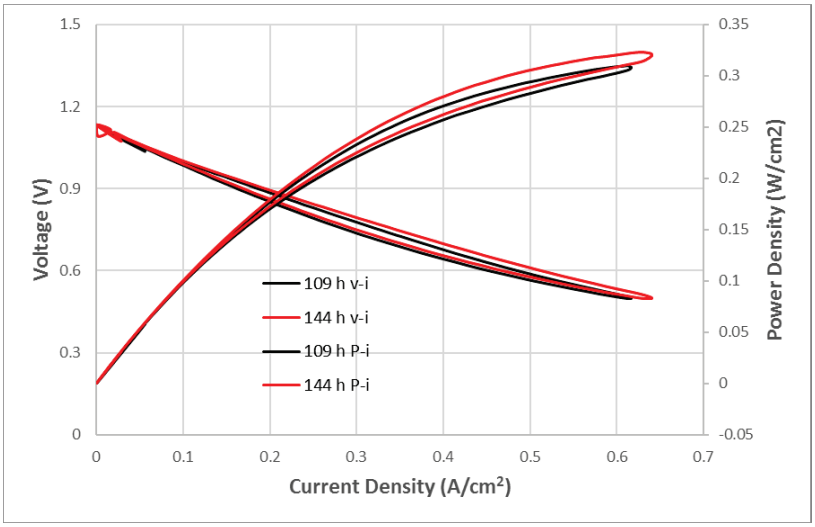

Figure 3 Comparison of the performance before and after the pause of the current load. Upon the pause of the current load, the cell performance is partially recovered.

This indicates that a certain degree of Cr accumulation could be reversible by regulating the oxygen partial pressure by means of changing the current load. It is expected that the Cr deposited on the LSM or ionic conductor surface during the oxygen reduction procedure under current load can be vaporized and removed from the cathode surface when the current load is removed and when the oxygen partial pressure is increased. However, as shown in Figure 2, in comparison with the cell initial performance, there are large decreases of the cell power density that cannot be recovered.

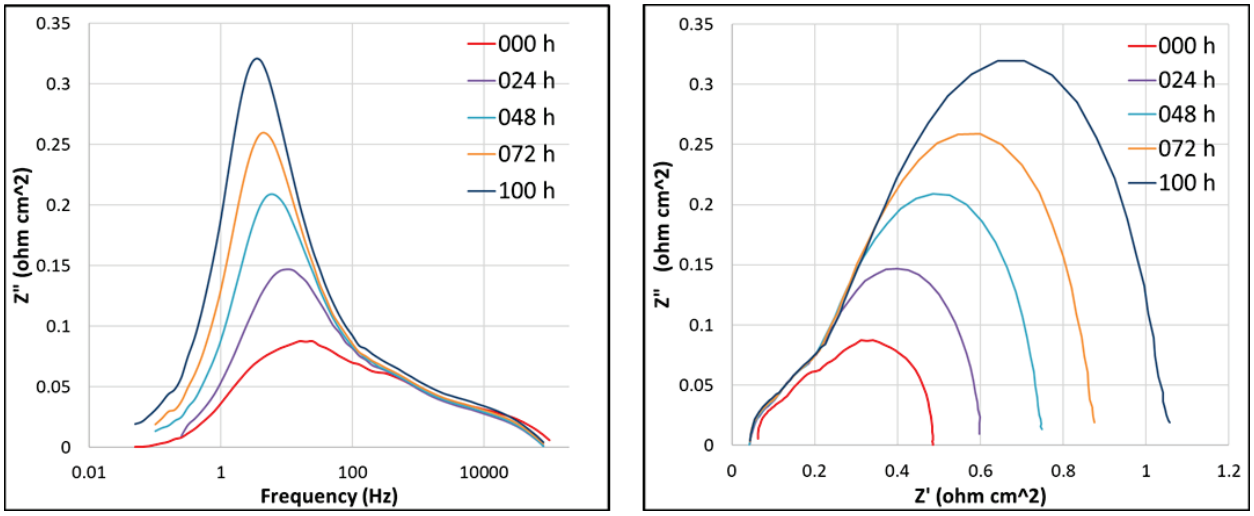

Figure 4 Impedance data for the LSM cell operated at 750 oC with Cr contamination.

After electrochemical operation, there is little change of series resistance Rs. However, there is large increase of the polarization resistance Rp. Rp increase could related to activity loss of oxygen reduction reaction at TPB.

4.4 Impact of Cr Contamination on the Nanostructure of Cathode

Upon the electrochemical operation, the above cell that has been electrochemically characterized are subjected to the TEM analysis. The cause of the irreversible component of the performance degradation was subjected to the nanostructure analysis of the above cell after the electrochemical operation for 109 h. The typical structure of the baseline shows the intact clean LSM/SSZ interface. In addition, there is no formation of the nano-scale MnOx, SrOx, or La2O3 phases. The internal surface of the pores is free of secondary phase.[17]

By contrast, the nanostructure of the LSM cell exhibits significant nanostructure changes upon operation with Cr contamination on the cathode.

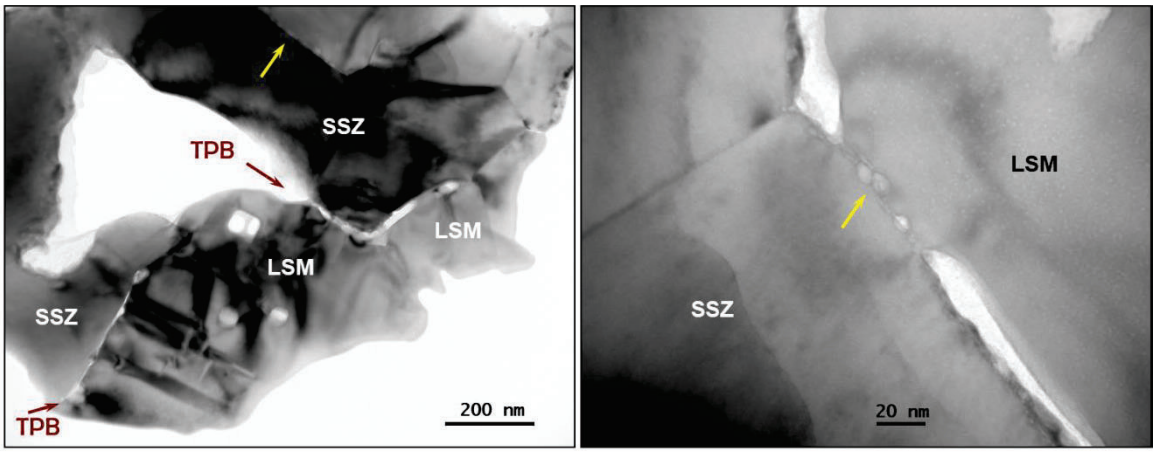

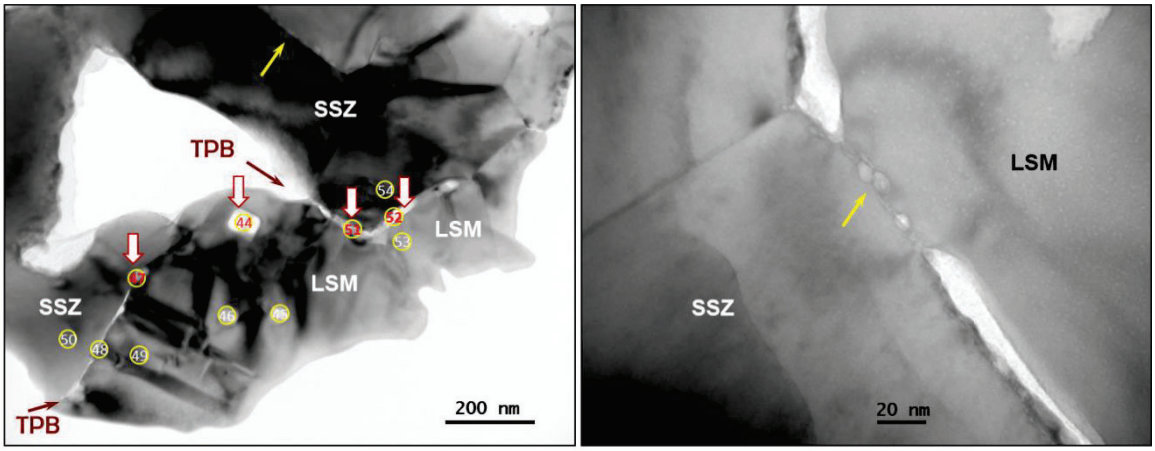

Atomic%	O	La	Sr	Mn	Zr	Sc	Cr	Formulation
44	66.37	12	3.1	15.14			3.39	$La_{0.79}Sr_{0.21}MnCr_{0.22}O_x$
45	71.89	10.37	2.53	14.76			0.46	$La_{0.8}Sr_{0.2}Mn_{1.14}Cr_{0.04}O_x$
46	68.01	11.99	3.23	16.65			0.12	$LaSrMn_{0.97}Cr_{1.06}O_x$
47	73.06	7.35		7.15	3.85	0.79	7.8	$LaSrMn_{0.97}Cr_{1.06}O_x + ZrO_2$ (w 10 % Sc_2O_3)
48	69.81	2.76		3.45	19.29	3.48	1.21	$LaSrMn_{1.25}Cr_{.44}O_x + ZrO_2$ (w 9 % Sc_2O_3)
49	71.34	10.66	2.69	15.31				$La_{.8}Sr_{.2}Mn_{1.15}O_x$
50	63.35			0.82	29.84	6		ZrO_2 (w 9 % Sc_2O_3) +Mn.03
51	70.96	2.7		4.14	7.43	1.75	13.04	CrOx enriched
52	76.77	2.73		2.94	12.46		5.11	CrOx enriched
53	73.19	9.96	2.44	12.78			1.63	$La_{.8}Sr_{.2}Mn_{1.03}Cr_{.13}O_x$
54	66.96			0.96	27.55	4.54		

Figure 5 Cr contaminants accumulated at the original TPBs and attack the internal interface between LSM and ionic conductor.

As shown in Figure 5, after operation with Cr contaminants, on the cathode, the internal cracking initiated from the original triple phase boundary (TPB) and propagated along the internal interface between Sc-stabilized ZrO2 (SSZ) and LSM. The end of the propagation path is Cr enriched.

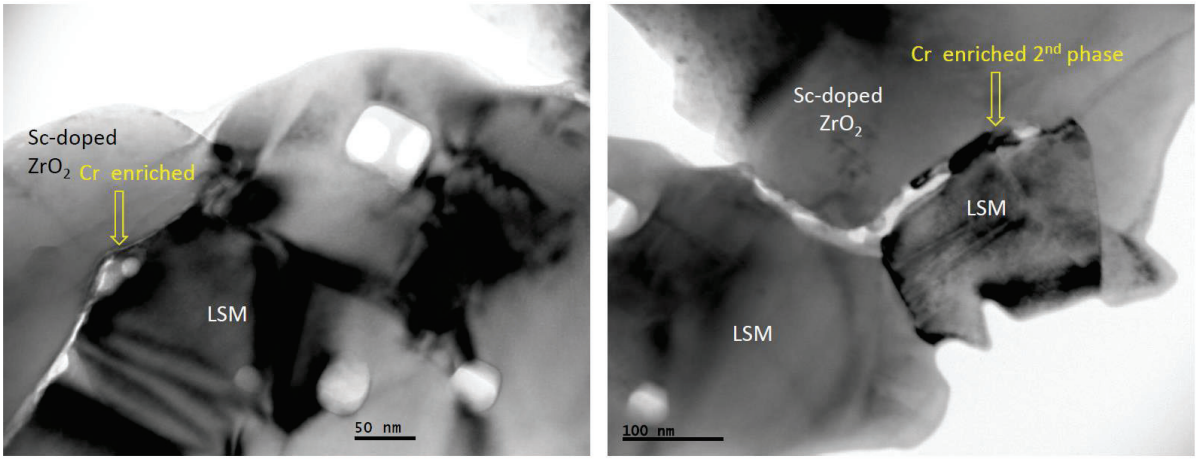

Figure 6 Cr contaminants cause the degradation of the LSM intragranular structure and the formation of the Cr-

enriched 2nd phase at the LSM and SSZ.

In the local SSZ/LSM interface region that there is no apparent internal cracking, there are internal nano-pores that are elongated along the SSZ/LSM interface. Intragranular structure has spherical nano-pores, while the SSZ grains remained to be intact, as shown in Figure 6.

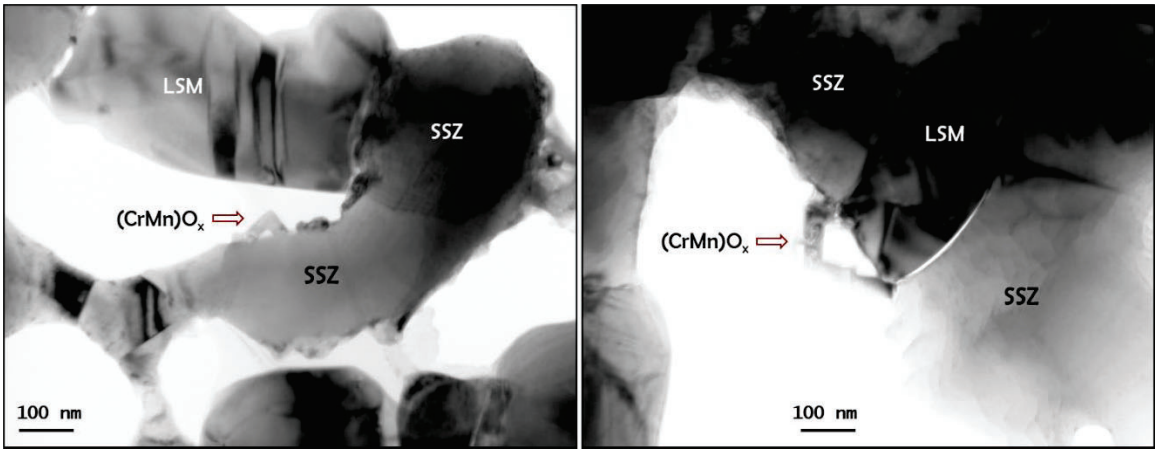

Figure 7 Formation of (CrMn)Ox on SSZ

Original TPB Degradation & Formation of (CrMn)Ox on SSZ grain surfaces. Additional (CrMn)Ox enriched crystals appear to nucleated at the original TPBs, as shown in Figure 7. Additional (CrMn)Ox enriched crystals appear to grow on SSZ grain surfaces.

For cathode contamination, the main cause for the Cr volatility is the thermodynamic instability of the chromia scales formed on the chromia forming alloys at high temperatures, forming gaseous species through the following reactions. [18,19]

Cr_2O_3 (s) + xO_2 (g) -> 2CrOi (g) (i ¼ 1, 2, 3)

Cr_2O_3 (s) + xO_2 (g) + yH_2O (g) -> 2Cr(OH)j (g) (j ¼ 3, 4, 5, 6)

Cr_2O_3 (s) + xO_2 (g) + yH_2O (g) -> $2CrO(OH)_n$ (g) (n ¼ 1, 2, 3, 4)

Cr_2O_3 (s) + xO_2(g) + yH_2O (g) -> $2CrO_2(OH)_k$ (g) (k ¼ 1, 2)

The volatile Cr species from the chromia scale strongly depend on the partial pressure of oxygen and the water content. Under current load, Cr was mainly detected within the active layer at the electrode and electrolyte interface and the Cr concentration increases significantly with the increase of the polarization current.[20]

For LSM based cathodes, the general microstructure observations due to the Cr contamination is the Cr accumulation at the LSM/YSZ interface region. [18]

O_2 (g) + $4e^-$ -> $2O^{2-}$

$2CrO_3$ (g) + $6e^-$ -> Cr_2O_3 (s) + $3O^{2-}$

$2CrO_2(OH)_2$ (g) + 6e <-> Cr_2O_3 (s) + $2H_2O$ (g) + $3O^{2-}$

Upon the electrochemical operation and the oxygen reduction reaction, the Cr volatized species deposited to the original TPB region that has reduced oxygen partial pressure. The electrochemical reduction of high valent Cr species would lead to the dominant formation of solid Cr_2O_3 at the LSM/YSZ interface. Meanwhile, the deposition of Cr on the LSM surface or on the YSZ/SSZ ionic conductor surface (other than TPB areas) would be kinetically very slow.

The distribution of Cr does not necessarily locate exactly at triple-phase boundaries (TPBs). Chemical deposition (i.e. with no electrochemical polarization reaction) of Cr2O3 can occur and is affected by the substrate material, which may be due to thermodynamic and/or catalytic properties of the electrode material. Nevertheless, under normal cathodic polarization potentials, there is no conclusive evidence for the actual decomposition of the LSM structure at the TPB region.[19,21,22]

4.5 Conclusion

The above nanostructure degradation analysis performed through this project is the first thorough analysis on the impact of the Cr contamination on the nanostructure of LSM/SSZ composite electrode of the SOFC cell upon electrochemical operation under industry relevant conditions.

For this present study, for the baseline cell, 100 h operation, the terminal voltage dropped ~ 190 mV. At 0.3 A/cm2; the baseline cell exhibits degradation rate is 1.68 V per 1000 h. After electrochemical operation, there is little change of series resistance Rs. However, there is large increase of the polarization resistance Rp. Previous literature report documented the deposition of the Cr species on the pore surface and the original TPB region. However, there is no reports on the Cr attacks of the LSM/SSZ internal interface and the LSM/LSZ grain boundaries. Such LSM/SSZ

internal interface degradation will cause the loss of the original TPBs and resulted in the increase of the polarization resistance. Meanwhile, the LSM/YSZ internal interface and LSM/LSM grain boundaries degradation are contributing to the increased Ωic resistance. Both the loss of the TPBs and degradation of the internal LSM/YSZ interface are the irreversible component of the degradation.

Even after the short period operation of 144 h at 750 ºC, there are irreversible nanostructure degradation occurs on the following regions: (1). Cr-Mn enriched nanograins deposited at the internal surface of the pore. Those Cr- enriched nano-grains are either amorphous or crystalline and with the dimension of the ~ 100 nm. Those Cr enriched grains are either on the SSZ ionic conductor surface or adjacent to the original TPB regions. The exact chemistry of the Cr-enriched nano-grains varies slightly. (2). Cr-enriched phase is present at the original TPB region and penetrates along the internal LSM/SSZ interface. The LSM/YSZ interface is with both voids and the nano-scale crystalline phase. The Cr has some solubility in LSM grains, there are ~ 50nm pores in the LSM grains. The major degradation is along the LSM/YSZ interface and the propagation length could be ~ 400 nm initialed from the original TPB region. (3). Cr-enriched phase is present at the original TPB region and penetrates along the internal LSM/LSM grain boundaries. Similar to the LSM/SSZ interface, the LSM/LSM grain boundaries are also with degradation. Such degradation is propagated deeply through the internal grain boundaries for about 200 nm in length. (4). Cr-enriched phase present at the SSZ surface grain boundaries. Except for the mechanical deposition, the Cr enriched phase does not appear to be able to penetrate the SSZ grains or the SSZ/SSZ grain boundaries. In comparison to the LSM that is vulnerable to Cr contamination at both the LSM grains and the grain boundaries, the SSZ or the ZrO2 ionic conductor appear to be Cr tolerant.

4.6 References

1 Badwal, S.; Deller, R.; Foger, K.; Ramprakash, Y.; Zhang, J., Interaction between chromia forming alloy interconnects and air electrode of solid oxide fuel cells. *Solid State Ionics* 1997, *99* (3-4), 297-310.

2 Chen, X.; Zhen, Y.; Li, J.; Jiang, S. P., Chromium deposition and poisoning in dry and humidified air at (La0. 8Sr0. 2) 0.9 MnO3+ δ cathodes of solid oxide fuel cells. *international journal of hydrogen energy* 2010, *35* (6), 2477-2485.

3 Jiang, S. P.; Chen, X., Chromium deposition and poisoning of cathodes of solid oxide fuel cells–a review. *International Journal of Hydrogen Energy* 2014, *39* (1), 505-531.

4 Park, E.; Taniguchi, S.; Daio, T.; Chou, J. T.; Sasaki, K., Influence of cathode polarization on the chromium deposition near the cathode/electrolyte interface of SOFC. *International Journal of Hydrogen Energy* 2014, *39* (3), 1463-1475.

5 Yang, Z.; Xia, G.-G.; Li, X.-H.; Stevenson, J. W., (Mn,Co)3O4 spinel coatings on ferritic stainless steels for SOFC interconnect applications. *International Journal of Hydrogen Energy* 2007, *32* (16), 3648-3654.

6 Nima Shaigan, Wei Qua, Douglas G. Ivey, Weixing Chen, A review of recent progress in coatings, surface modifications and alloy developments for solid oxide fuel cell ferritic stainless steel interconnects*, Journal of Power Sources* 195 (2010) 1529–1542.

7 Taniguchi S, Kadowaki M, Kawamura H, Yasuo T, Akiyama Y, Miyake Y, et al. Degradation phenomena in the cathode of a solid oxide fuel cell with an alloy separator. J Power Sources 1995;55:73e9.

8 Horita T, Xiong Y, Kishimoto H, Yamaji K, Brito ME, Yokokawa H. Chromium poisoning and degradation at (La,Sr) MnO3 and (La,Sr)FeO3 cathodes for solid oxide fuel cells. J Electrochem Soc 2010;157:B614e20

9 VOHS, J. M. & GORTE, R. J. 2009. High-Performance SOFC Cathodes Prepared by Infiltration. *Advanced Materials,* 21, 943-956.

10 CRACIUN, R., PARK, S., GORTE, R. J., VOHS, J. M., WANG, C. & WORRELL, W. L. 1999. A Novel Method for Preparing Anode Cermets for Solid Oxide Fuel Cells. *Journal of The*

Electrochemical Society, 146, 4019-4022.

[11] KIM, H., LU, C., WORRELL, W. L., VOHS, J. M. & GORTE, R. J. 2002. Cu-Ni Cermet Anodes for Direct Oxidation of Methane in Solid-Oxide Fuel Cells. *Journal of The Electrochemical Society,* 149, A247-A250.

[12] GORTE, R. J., PARK, S., VOHS, J. M. & WANG, C. H. 2000. Anodes for direct oxidation of dry hydrocarbons in a solid-oxide fuel cell. *Advanced Materials,* 12, 1465-1469.

[13] HE, H. P., HUANG, Y. Y., REGAL, J., BOARO, M., VOHS, J. M. & GORTE, R. J. 2004. Low-temperature fabrication of oxide composites for solid-oxide fuel cells. *Journal of the American Ceramic Society,* 87, 331-336.

[14] LEE, S., MILLER, N., STARUCH, M., GERDES, K., JAIN, M. & MANIVANNAN, A. 2011. $Pr_{0.6}Sr_{0.4}CoO_{3-delta}$ electrocatalyst for solid oxide fuel cell cathode introduced via infiltration. *Electrochimica Acta,* 56, 9904-9909.

[15] LEE, S., MILLER, N. & GERDES, K. 2012. Long-Term Stability of SOFC Composite Cathode Activated by Electrocatalyst Infiltration. *Journal of the Electrochemical Society,* 159, F301-F308.

16 Jiang, S. P. & Chen, X. Chromium deposition and poisoning of cathodes of solid oxide fuel cells – a review. *Int. J. Hydrog. Energy* 39, 505–531 (2014).

17 Chen, Yun, Yueying Fan, Shiwoo Lee, Gregory Hackett, Harry Abernathy, Kirk Gerdes and Xueyan Song. "Interface and Grain Boundary Degradation in Lsm-Ysz Composite Solid Oxide Fuel Cell Cathodes Operated in Humidified Air." Journal of Power Sources 438, (2019): 227043

18 K. Hilpert, D. Das, M. Miller, D. Peck, R. Weiss, Journal of the Electrochemical Society, 143 (1996) 3642.

19 S.P. Jiang, X. Chen, International Journal of Hydrogen Energy, 39 (2014) 505-531.

20 E. Konysheva, H. Penkalla, E. Wessel, J. Mertens, U. Seeling, L. Singheiser, K. Hilpert, Journal of the Electrochemical Society, 153 (2006) A765-A773.

21 S.P. Jiang, W. Wang, Electrochemical and Solid-State Letters, 8 (2005) A115.

22 J.W. Fergus, International Journal of Hydrogen Energy, 32 (2007) 3664-3671.

5 ALD Enabled Chromium Tolerant, Highly Active & Stable LSM Cathodes

5.1 ALD coating & its technical challenges for infiltrating Cr-tolerant layer on SOFC cathode

5.1.1 Enhanced Cr tolerance through solution based infiltration

The mechanism of the Cr deposition process described above implies that an electrode surface coating layer, which is inert to Cr inward diffusion to cathode could act as barrier layer to prevent the direct reaction between the Cr with electrode, and enhance the Cr tolerance. For example, for the LSCF/SDC composite electrode, there is evidence that solution-based cathode infiltration[1,2,3,4,5,6,7] of chromium inert phases, such as ionic-conducting $Ce_{0.9}Gd_{0.1}O_{2-d}$ (GDC), could mitigate the Cr poisoning [8]. The impregnated GDC nano-particles may act as a buffer layer to prevent the direct contact between LSCF and chromium species, improving the cathode tolerance towards Cr deposition.

From the structure point of view, the Cr-tolerant surface coating layer on the SOFC cathode needs to be: (1). ***Deeply penetrating into the active layer*** of the cathode. (2). ***Uniform and conformal*** on the internal surface of the cathode active layer that possess complex three-dimensional topographies with high aspect ratio. (3). ***Intimate adhesion and bonding*** to the cathode surface at atomic scale without spallation.

Magnetron sputtering, sol-gel dip-coating, and electrodeposition techniques are used for applying protective coating on ferritic stainless-steel interconnects. Those deposition techniques involve physical vapor deposition or liquid solutions. None of those interconnect coatings will be ideal for infiltrating the cathode surface, since they have the limitation of not deeply penetrating into the cathode active layer or not providing the conformal coating on cathode surface.

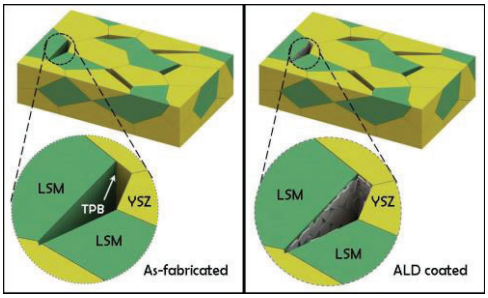

Fig. 1 Schematic of conformal ALD coating of LSM/YSZ developed by PI.

5.1.2 PI's work on development of highly active & stable ALD coating layer on SOFC cathode

The ALD coatings developed by the PI are uniform and

conformal covering the entire internal surface of the porous cathode. PI's work has demonstrated that the ALD coating layer, applied on the internal surface of LSM/YSZ porous cathode, could be ionic conductor[9], electronic conductor, electrochemical catalyst, and the catalytic noble metal. Thus, the surface morphology and the function of the deposited layer can be precisely tailored. In term of the Cr-poisoning, such conformal ALD layer could coat protective layer on specific locations, such as the TPBs, that are vulnerable sites to the Cr vapor deposition, as shown in Fig.1.

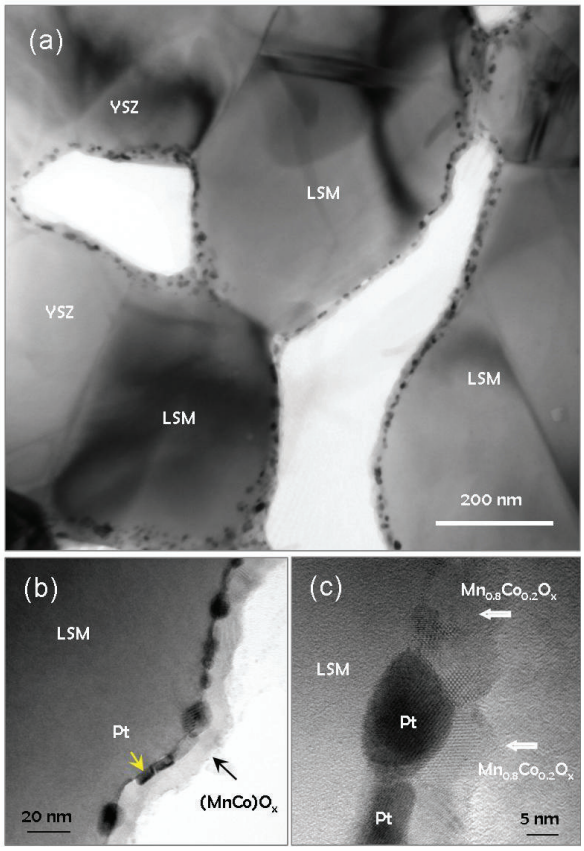

Fig. 2 (a). Stable surface ALD architecture after cell operation for 120 h at 750℃.

The PI of this proposal continuously designed the electrode internal surface nanostructure using ALD infiltration. As part of the PI's ***pending patent***, for the first time in the field of fuel cell, PI has demonstrated the establishment of the **mesoporous nanoionics** for high temperature SOFC applications. The designed stable mesoporous nanoionics have resulted in the performance enhancement for state-of-the-art commercial cells by a factor of 1.5-1.7, the highest performance enhancement ever reported for SOFC until the year 2016. This part of the work has been well documented in a recent paper[9] entitled "Nanoionics and Nanocatalysts: Conformal Mesoporous Surface Scaffold for Cathode of Solid Oxide Fuel Cells" published in "Scientific Reports" from Nature Publishing Group. Very recently, the PI has demonstrated the formation of a new architectures enabled by ALD coating of LSM/YSZ cathode and resulted in cell performance enhancement by a factor of 3.7 for commercial cells operated at 750°C. Dual-layer ALD coating of ~ 5 nm Pt first, subsequently followed by ALD coating of 15 nm thick $(Mn_{0.8}Co_{0.2})_3O_4$ was applied on the LSM/YSZ cathode of commercial

cells. This is simple one step processing of as-received cells, and the change of the chemistry in ALD layer was achieved through computer controlled automatic switching of the precursors. No heat-treatment was applied before or after ALD coating, and the cell electrochemical operation was carried out directly after ALD coating.

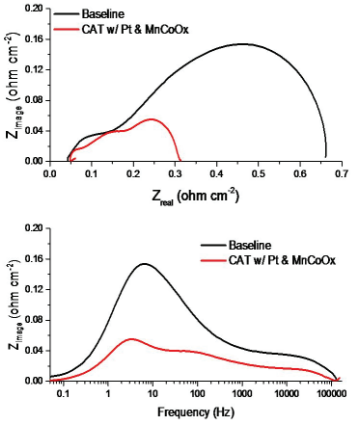

Fig. 2(c). Decrease of the polarization resistance induced by ALD dual layer.

The dual-layer coating nano-composite appears to be remarkable stable upon cell operation. After 120 h operation at 750 °C, the surface layer is conformal and ALD layer thickness is uniform over the entire internal surface of the LSM/YSZ cathode, as shown in Fig. 2 (a). Size and distribution of nano-grains are also uniform within the ALD coating layer on both the LSM and YSZ grain surface. Superjacent layer is continuous layer of $(Mn_{0.8}Co_{0.2})_3O_4$ with nano-grains and nano-pores, both with dimension of ~ 10 nm. The superjacent $(Mn_{0.8}Co_{0.2})_3O_4$ is apparently pinning the Pt, resulting in the subjacent layer with dense & uniform ~5-10 nm Pt on LSM/YSZ, as schematic shown in Fig. 2(b).

It is worthwhile to point out that Pt is stabilized as uniform and man-sized on both the LSM and YSZ grain surface. Pt coarsening is consistently reported by the researchers[10,11] Pt is found deposited solely at original TPB region, where the oxygen partial pressure is lowest. In the present study, the distribution of high-density nano-Pt indicates the instantaneous formation of the TPBs on both LSM and YSZ surface, facilitated by the continuous layer of $(Mn_{0.8}Co_{0.2})_3O_4$ nano grains.

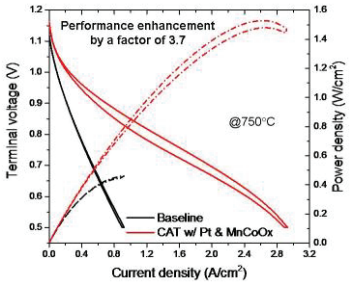

Fig. 2 (d). Performance enhancement by a factor of **3.7**, induced by **ALD dual layer**.

Such a dual-layer composite has resulted in significant reduction of the polarization resistance as shown in Fig. 2 (c) and the dramatic performance enhancement for the cell power density **by a factor of 3.7**, as shown in Fig. 2 (d), and Table 1. This dramatic performance enhancement is strongly related to the unique design of the

Table. 1 Performance enhancement by a factor of 3.72.

	R_{total} ohm cm^{-2}	R_s ohm cm^{-2}	R_p ohm cm^{-2}	i at 0.8 V A cm^{-2}	P at 0.8 V W cm^{-2}	Factor of enhancement
LSM/YSZ Baseline	0.661	0.043	0.618	0.355	0.284	1
ALD/Pt, & $(MnCo)_3O_4$	0.311	0.048	0.263	1.32	1.056	**3.72**

nanostructured ALD layer. Because of the thinness of the superjacent $(Mn_{0.8}Co_{0.2})_3O_4$ layer, which is essentially an excellent electronic catalyst and electronic conductor facilitating *faster oxygen exchange*, and the existence of the nano-pores within the ALD layer, the subjacent Pt particles on the surface of ionic conductor YSZ are all fully activated for electrochemical reactions. Such activation is achieved by (1) accelerating dissociative adsorption of oxygen molecules on the Pt surface; and (2) accelerating surface diffusion of adsorbed oxygen atoms to the TPBs of Pt-$(Mn_{0.8}Co_{0.2})_3O_4$-YSZ-air. When the electroactive oxygen is reduced along the entire interface between gas exposed Pt and $(Mn_{0.8}Co_{0.2})_3O_4$, it quickly diffused from the TPB along the adjacent Pt/YSZ interface. The above two effects were maximized due to high surface area owing to the presence of nano-sized particles. In short, due to the ALD dual layer coating, in addition to the original TPBs, the YSZ surface that is originally not the site for the electrochemical reactions, has become the rapid pathway for both oxygen reduction reactions and electrochemical reactions and resulted in the large performance enhancement.[12,13,14] On the other hand, on LSM backbone, there are three electrocatalysts, namely LSM, $(Mn_{0.8}Co_{0.2})_3O_4$ and Pt surfaces, to contribute ORR simultaneously.

5.2 Experimental section

Commercially available, anode-supported solid oxide button cells fabricated by CTG (Salt Lake City, UT) were employed for all the experiments described in this paper. MSRI cells are composed of five layers as follows, starting from the anode: a ~700 μm thick Ni/YSZ cermet layer which supports the cell structure; a ~10 μm thick Ni/YSZ active layer; a ~10 μm thick YSZ electrolyte; a thin (2-3 μm), dense Sm_2O_3-doped CeO_2 (SDC) barrier layer, a ~10 μm thick LSM/YSZ or LSM/SSZ active layer; and a 50 μm thick, pure LSM current collecting layer. The cell active area (limited by the cathode) is 2 cm^2. The exposure area of the anode to fuel is about 3.5 cm^2.

The ALD coatings were performed in a commercial GEMStar-8 ALD reactor from Arradiance Inc. No masking or specific treatment is applied on the NiO/YSZ anode before ALD processing. The thick and very dense NiO/YSZ anode prevents precursor penetration during the ALD processing,

and the impact of ALD coating on the Ni/YSZ anode is negligible. No surface pretreatment or heat-treatment was applied before or after ALD coating either. The cell electrochemical operation was carried out directly after the ALD coating.

A set of experiments were carried out in a Cr-rich environment and a different set of samples were analyzed in a Cr-free environment to see the influence of Cr in the air electrodes of the cell. Inconel 600 mesh was used as Cr source to create a Cr-rich environment in the air electrode side. The active area of the cells is limited by the cathode, as such both the power density and current density are calculated considering this area even if the anode exposure to fuel is larger in area than the active area of the cathode. In our test, the LSM/SSZ button cell as-fabricated by CTG was subject to operation on a single cell test station at 750 C under a Cr source for ~200 h. A multilayer-mesh stack was used as the inter-connect. The mesh stack includes 3 layers of Pt mesh and two layers of Inconel 600 mesh. The chemical composition of Inconel 600 used in this study is Al ~0.2, Co 0.03, Cr 16.05, Fe 8.6, Mn 0.45, NI 73.7 Ti 0.21 and other 0.76 (all in wt %).

All cell tests were performed on a test stand. The platinum mesh was used for anode and cathode lead connections. The fuel and air stream flow rates were controlled separately using mass flow controllers. During the operation, a 400 mL/min air flow rate and a 400 mL/min fuel flow rate were used. Before any electrochemical measurements, both cells were current-treated for approximately ~15 h under a small current density of 0.1 A/cm^2 to ensure they were activated. After that, the samples were loaded at a constant current of 0.3 A/cm^2 for desired periods. The cell performance was examined using a TrueData-Load Modular Electronic DC Load, which guarantees voltage and current accuracies of 0.03 % FS of the range selected +/-0.05 % of the value. The cell impedance spectra were examined using a potentiostat/galvanostat (Solartron 1287A) equipped with a frequency response analyzer (Solartron 1260). Impedance measurements were carried out using a Solatron 1260 frequency response analyzer in a frequency range from 50 mHz to 100 KHz. The impedance spectra and resistance (Ωic resistance Rs and polarization resistance Rp) presented are those measured under a DC bias current of 0.3 A/cm^2. On a Nyquist plot, Rs is determined by the intercept at the higher frequency end, and Rp is determined by the

distance between two intercepts.

After the electrochemical operation, the ALD coated cells were sectioned and subjected to nanostructural and crystallographic examination using high resolution (HR) Transmission Electron Microscopy (TEM). All the TEM examinations were conducted in the cathode active layer. TEM samples were prepared by mechanical polishing and ion milling in a liquid-nitrogen-cooled holder. Electron diffraction, diffraction contrast, and HRTEM imaging were performed using a JEM-2100 operated at 200 kV. Chemical analysis was carried out under TEM using energy dispersive X-ray Spectroscopy (EDS).

5.3 Simultaneously improved performance and Cr tolerance induced by ALD

Upon the thorough analysis of the nanostructure origin of the LSM/YSZ cathode performance degradation induced by Cr contamination, we have focused on the development of Cr- tolerant cathode by applying the conformal ALD coatings with sufficiently ORR active and chemically/thermally stability.

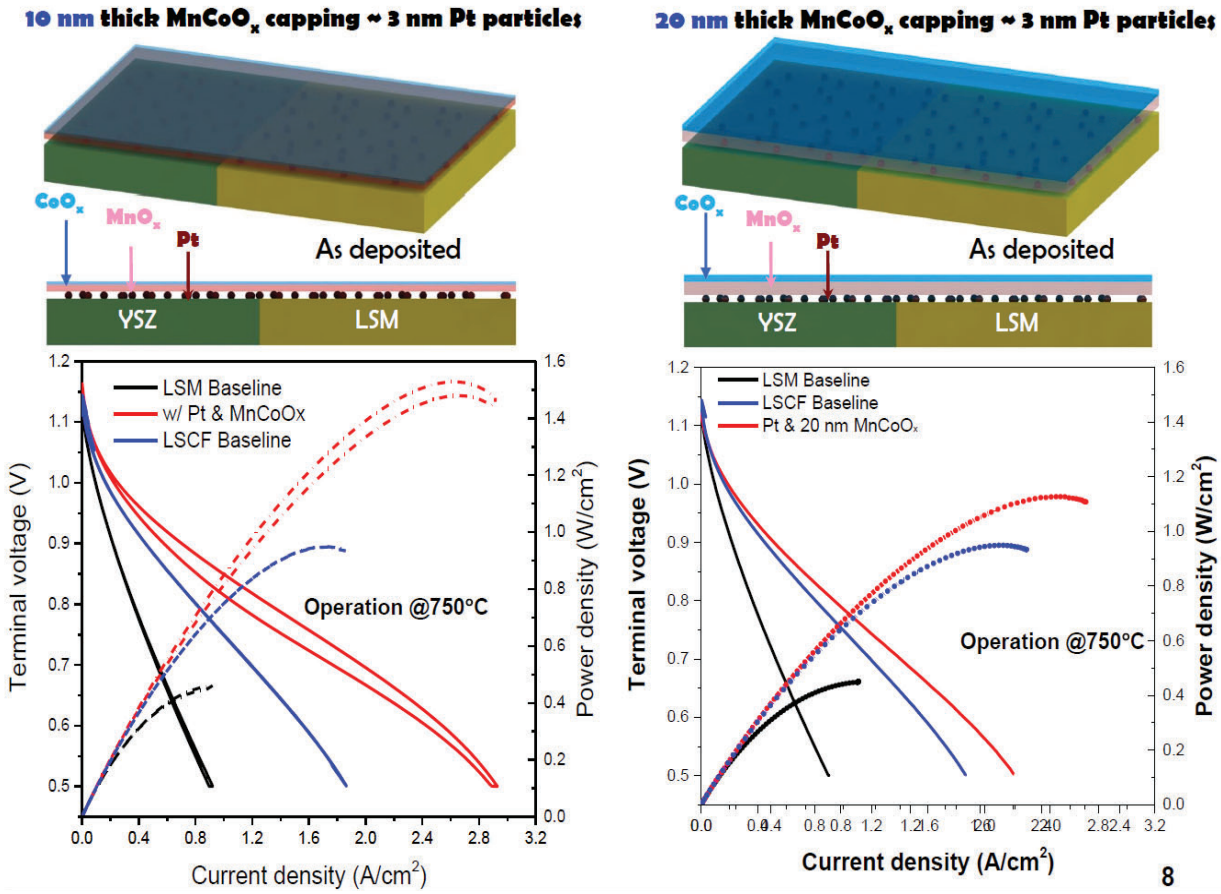

Fig. 3: The tunable cathode performance upon adjusting the thickness of the ALD layer. The unique feature of the ALD coating layer developed through this project include: (a). Highly active towards electrochemical reactions. (b). Super stable upon the long-term electrochemical operation at high temperatures. (c). Extremely robust towards Cr poisoning.

One of the first choices of ALD coating layer is the $Mn_{0.8}Co_{0.2}O_x$ that is the ordinary interconnect coating materials, and an excellent layer to prevent Cr penetration. For the $Mn_{0.8}Co_{0.2}O_x$/Pt dual layer composite, we have kept the subjacent Pt layer unchanged. When the superjacent is 10 nm thick $MnCoO_x$ capping ~ 3 nm Pt particles, the ALD coated cell the peak power density is 380 % of baseline. When the superjacent is 20 nm thick $Mn_{0.8}Co_{0.2}O_x$ capping ~ 3 nm Pt particles is 280 % of baseline. In order to have high Cr resistance, the cell with an ALD layer consisting of 20 nm thick $MnCoO_x$ capping layer is applied to the cell testing, as shown in Figure 3.

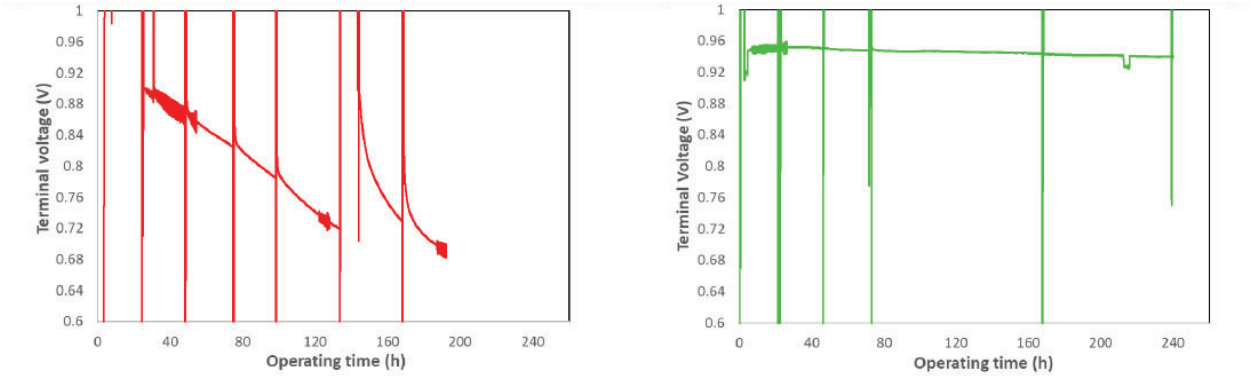

SSZ: Scandium stabilized ZrO_2
LSM/SSZ, baseline at 0.3 A/cm²
Degradation rate is 1.68 V per 1000 h

Operating time (h)	Peak power density (W/cm²)	Percentage degradation (%)
0	0.862	-
24	0.605	29.8 %
50	0.45	47.8 %
74	0.375	56.5 %
109	0.307	64.4 %

YSZ: Yttrium stabilized ZrO_2
ALD coated **LSM/YSZ** at 0.3 A/cm²
Degradation rate is 0.054 V per 1000 h

Operating time (h)	Peak power density (W/cm²)	Percentage degradation (%)
23	1.254	-
44	1.127	0.101276
68	1.073	0.144338
168	1.015	0.19059

Baseline Cell: Peak power density remained to be 36%, of baseline @ zero hour, after 109 hours operation.

ALD coated one: Peak power density remained to be 200%, of baseline @ zero hour, after 168 hours operation.

Cr tolerance: $Mn_{0.8}Co_{0.2}O_x$ is ordinary interconnect coating materials, excellent layer to **prevent Cr penetration**.

Figure 4 The direct comparison of the performance of the baseline cell and the ALD coated cells that were

operated under identical condition when the cathodes were put in contact with Cr-containing Inconel interconnect. As it is reported above, for the baseline Cell operated with the cathode in contact with Cr-containing Inconel interconnect, the cell peak power density remained to be 36 % of baseline @ zero hour, after 109 h operation. By contrast, ALD coating immediately boosts the cell power density to 280 % of baseline. Upon 168 h operation with the cathode in contact with Cr-containing Inconel interconnect, the ALD coated one is having Peak power density remained to be 200 % of baseline cell that is operated at hour. **As such, through this project, we have successfully demonstrated that ALD coating is highly active towards electrochemical reactions and Extremely robust towards Cr poisoning.**

5.4 Electrode Surface Modifications Integrate of ALD coating with Solution Infiltration

5.4.1 Repeating experiment of baseline cell performance degradation caused by Cr contamination

The electrochemical operation examinations at 750 °C of the sample corresponding to a baseline LSM-CTG subject to Cr contamination (with Inconel 600 as Cr source) cell are shown in Figure 1. The baseline LSM sample achieves a maximum initial peak power density of 0.862 W/cm^2 at 750 °C. Nonetheless, the performance decreases over time when the cell is being exposed to the Cr volatile species. The decrease in performance can be observed in Figure 4. The peak performances at different operation times are 0.605 W/cm^2 at 24 h, 0.450 W/cm^2 at 50 h, 0.375 W/cm^2 at 74 h, 0.307 W/cm^2 at 109 h, and 0.317 W/cm^2 at 144h. The percentage reduction in performance compared to baseline at 0h (0.862 W/cm^2) are 29.8% at 24 h, 47.8% at 50 h, 56.5% at 74 h, 64.3% at 109 h, and 63.2% at 144h. The results indicate the rapid decay in performance for the baseline LSM cell under Cr contamination. The Cr exposure leads to a reduction of 1.24%/h during the initial 24 h, 0.95%/h considering the first 50 h, and 0.58%/h for 109 h under Cr exposure for the SOFC operation at 750 °C. Furthermore, Table 1 shows the performance of the cells at the different V-I conditions.

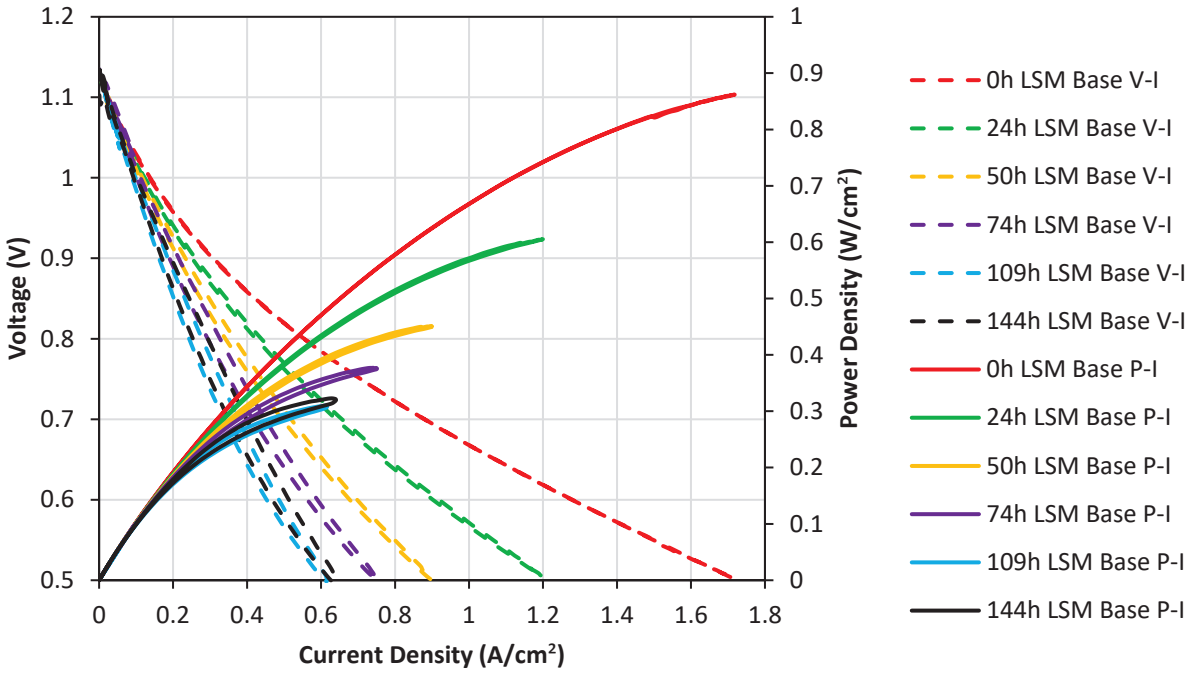

Figure 4: Typical I−V−P curves of the baseline LSM anode-supported solid oxide button cells showing the performance evolution for SOFC operation at 750 °C under Cr contamination.

Table 1: Numerical values obtained from the I−V−P curves at 750 °C for SOFC LSM baseline cell under Cr contamination.

Performance	0h		24 h		50 h		74 h		109 h		144h	
V(V)	I(A/cm²)	P(W/cm²)	I(A/cm²)	P(W/cm²)	I(A/cm²)	P(W/cm²)	I(A/cm²)	P(W/cm²)	I(A/cm²)	P(W/cm²)	I(A/cm²)	P(W/cm²)
0.5	1.718	0.862	1.200	0.605	0.899	0.450	0.750	0.375	0.616	0.307	0.637	0.317
0.6	1.287	0.769	0.932	0.550	0.679	0.407	0.569	0.339	0.457	0.273	0.473	0.282
0.7	0.920	0.634	0.647	0.451	0.496	0.347	0.419	0.292	0.339	0.237	0.352	0.246
0.8	0.572	0.454	0.446	0.352	0.357	0.282	0.296	0.236	0.245	0.195	0.255	0.204

5.4.2 Electro-Impedance performance evaluation of baseline

The impedance plots and data are shown in Figure 2 and Table 2, respectively. The impedance of the LSM baseline cell shows minimum values of R_s=0.0610 Ωcm^2 and R_p=0.4241 Ωcm^2, at 750 °C, as shown from the Nyquist plot in Figure 2b. There is an increase in the R_p values after the continuous SOFC operation under Cr volatile species. The R_p values of the LSM baseline cell at different operation times are 0.4241 Ωcm^2 at 0h, 0.5578 Ωcm^2 at 24 h, 0.7065 Ωcm^2 at 48h, 0.8332

Ωcm^2 at 72h, and 1.0101 Ωcm^2 at 100h. These values represent an increase on the Rp at different time frames of 31.5% at 24 h, 66.5% at 48h, 96.4% at 72 h, and 138.1% at 100 h.

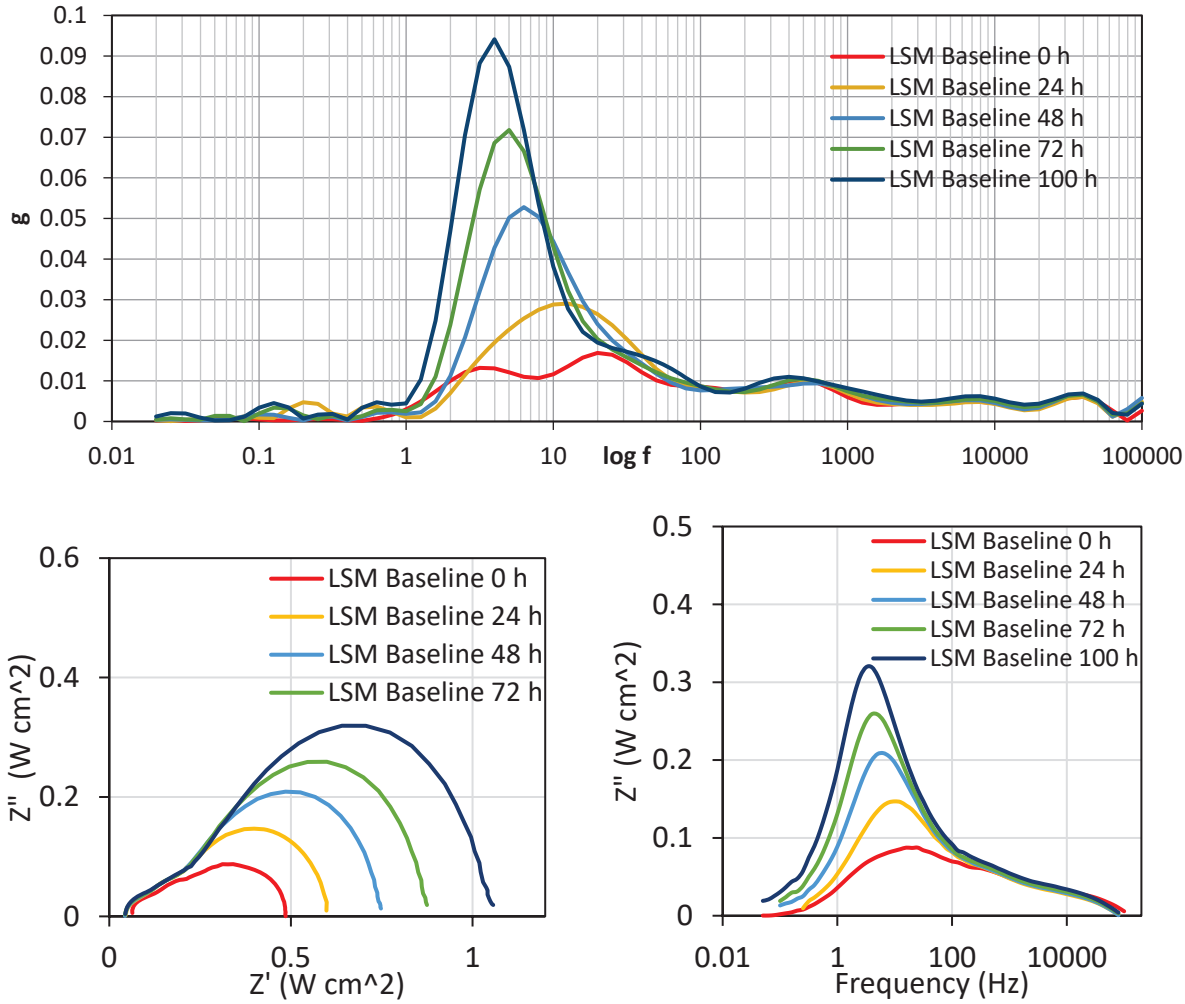

Figure 5: Impedance of the LSM anode-supported showing the impedance data at 750 °C for the SOFC operation under Cr contamination. Top: Deconvolution spectra of the impedance data collected from the different cells operated at 750 °C and 0.3A/ cm^2. Right bottom: Nyquist plots at 0.3 A/cm^2. Left bottom: Bode plots of cells at 0.3 A/cm^2.

As previously discussed, the power density on the LSM baseline cell deteriorates when the cell is subject to SOFC operation under Cr volatile species(with up to 64.3% reduction of performance after 109 h of operation). The LSM performance degradation could be attributed to the Cr deposition at the active sites of the air electrode LSM. As the Bode plots in Figure 2c shows,

the main increase in polarization resistance comes from the LSM air electrode. Notably, the LSM baseline cell does not show any significant increase in the Ωic resistance. Thus, the main degradation arises from the formation of the secondary phase in the air electrode, which blocks active sites for the oxygen reduction reaction, leading to a higher polarization resistance over time.

Figure 6 and Table 2 show the evolution of the Ωic and polarization resistance for the LSM anode-supported solid oxide button cell at different times of SOFC operation at 750 °C under Cr contamination.

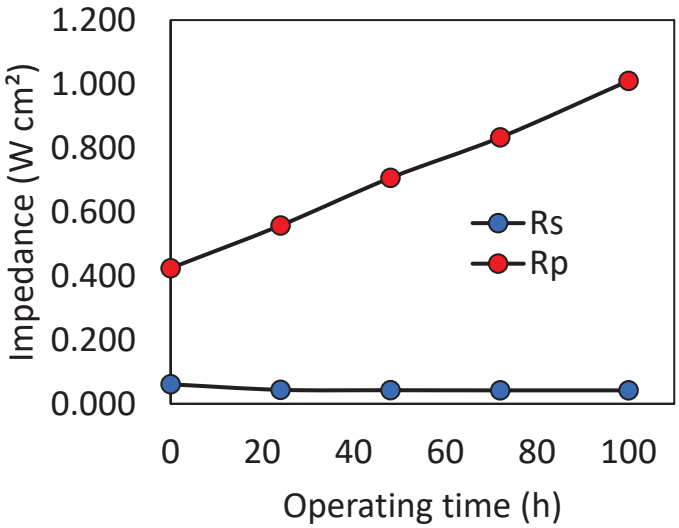

Figure 6: Evolution of ohmic (Rs) and polarization (Rp) resistance for the LSM anode-supported solid oxide button cell at different times of SOFC operation at 750 °C under Cr contamination.

Table 2: Numerical values obtained from impedance data of LSM baseline cell showing the Rs and Rp at different times of 750 °C SOFC operations under Cr contamination.

	LSM base 0h	LSM base 24 h	LSM base 48h	LSM base 72h	LSM base 100h
Rs (Ω cm²)	0.0610	0.0436	0.0425	0.0420	0.0420
Rt (Ω cm²)	0.4852	0.6014	0.7490	0.8753	1.0521
Rp (Ω cm²)	0.4241	0.5578	0.7065	0.8332	1.0101

Figure 7 shows the evolution of the terminal voltage when the LSM baseline cell is operated at a constant current density of 0.3 A/cm^2 in SOFC mode under Cr contamination. The data from the terminal voltage plot shows the voltage degradation at different timeframes. For the SOFC operation under Cr volatile species, the voltage at different times is 0.900 V at 0h of SOFC operation, 0.872 V at 25h, 0.824 V 50 h, 0.795 V 74 h, and 0.719 V at 109 h of SOFC operation.

These values represent a reduction in voltage of 28mV at 25h(1.12mV/h) or (0.12%/h); 76mV at 50 h (1.52mV/h) or (0.16%/h); 105mV at 74 h (1.42mV/h) or (0.15%/h); and 181mV at 109 h (1.66mV/h) or (0.18%/h). Thus, it can be concluded that the V drop for the SOFC operation with exposure to a Cr source when subject to a current density of 0.3A/cm2 is 1.66mV/h of operation or 0.18%/h of operation. For the LSM baseline cell operated for 109 h under Cr exposure, the reduction corresponds to 20%. Table 3 shows the values obtained from the terminal voltage data for the different SOFC parameters at different operation times.

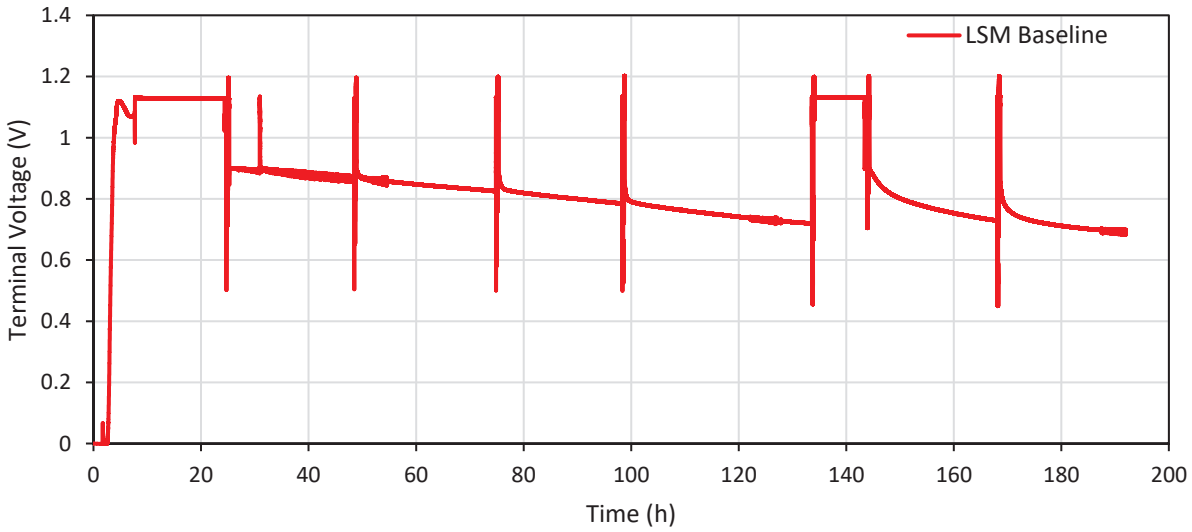

Figure 7: Evolution of terminal voltage when the LSM baseline cell is operated at a constant current density of 0.3 A/cm2 in SOFC mode under Cr contamination. The peaks on the graph corresponded to the timeframe when impedance and power density analysis was taken.

Table 3: Numerical values obtained from terminal voltage data of LSM baseline cell showing voltage drop when the cell is operated at a constant current of 0.3 A/cm^2 in SOFC mode with Cr contamination.

LSM Baseline SOFC w/Cr source					
Time SOFC operation	Peak P(W/cm^2)	Peak ΔP (%)	I(A/cm^2)	V(V)	ΔV (mV) [% drop]
0	0.862	0	0.3	0.900	0 [0]
25h	0.605	29.8	0.3	0.872	28 [3.0]
50 h	0.450	47.8	0.3	0.824	76 [8.4]
74 h	0.375	56.5	0.3	0.795	105 [11.6]
109 h	0.307	64.3	0.3	0.719	181 [20.1]

5.4.3 Infiltration and ALD Mn and Co SOFC 750°C operation with Cr source (In600)

The electrochemical operation examinations at 750 °C of the sample corresponding to an

LSM-CTG cell infiltrated with Pr via dip coating and coated with Mn and Co via ALD are shown in Figure 5. The LSM PrMnCo sample achieves a maximum initial peak power density of 0.810 W/cm^2 at 750 °C. The performance does not have to suffer any significant deterioration when the cell is being exposed to the Cr volatile species. The evolution of performance at different operation times can be observed in Figure 8. The peak performances at different operation times are 0.8103 W/cm^2 at 0h, 0.7361 W/cm^2 at 27 h, 0.8093 W/cm^2 at 168 h, and 0.8225 W/cm^2 at 240 h. The percentage change in performance compared to baseline at 0h (0.8103 W/cm^2) are -9.1% at 27 h, -0.1% at 168 h, and +1.5% at 240 h. The results indicate that the infiltrated and ALD coated Mn and Co cell does not suffer degradation in performance under Cr contamination. There is some initial degradation but after 240 h of operation, the cell still shows a similar performance to the initial values. Furthermore, Table 5 shows the performance of the cells at the different V-I conditions.

Table 4: Numerical values obtained from the I−V−P curves at 750 °C for SOFC LSM cell infiltrated with via dip coating and coated with Mn and Co via ALD under Cr contamination.

Performance	0 h		27 h		168 h		240 h	
V(V)	I(A/cm^2)	P(W/cm^2)	I(A/cm^2)	P(W/cm^2)	I(A/cm^2)	P(W/cm^2)	I(A/cm^2)	P(W/cm^2)
0.5	1.604	0.805	1.467	0.735	1.613	0.809	1.640	0.822
0.6	1.297	0.774	1.137	0.682	1.248	0.745	1.257	0.751
0.7	0.965	0.671	0.837	0.583	0.877	0.615	0.881	0.619
0.8	0.637	0.509	0.557	0.446	0.569	0.457	0.570	0.459

The ASR values for the LSM cell infiltrated via dip coating and coated with Mn and Co via ALD are shown in Table 5. The LSM surface-modified cell shows an initial ASR value of 0.3602 Ωcm^2 at 750 °C. The evolution of the ASR values at different times shows that there is no significant degradation after 240 h of SOFC operation under Cr volatile species. The ASR value after SOFC operation under Cr exposure display an initial 10.1 % increase at 27 h but the subsequent 2.2 % reduction at 240 h.

Table 5: Numerical values obtained from the I−V−P curves at 750 °C for SOFC LSM cell infiltrated with dip coating and coated with Mn and Co via ALD under Cr contamination.

	0h	27 h	168 h	240 h

ASR (Ω cm^2)	0.3602	0.3967	0.3565	0.3523

The impedance plots and data are shown in Figure 6 and Table 6, respectively. The impedance of the LSM cell infiltrated with dip coating and coated with Mn and Co via ALD shows minimum initial values of R_s=0.0676 Ωcm^2 and R_p=0.4033 Ω cm^2, at 750 °C, as shown from the Nyquist plot in Figure 6b. There is very small increase in the R_p values after the continuous SOFC operation under Cr volatile species. The LSM cell infiltrated with dip coating and coated with Mn and Co via ALD cell shows R_p changes at different operation times with values for R_p (R_s) of 0.4410(0.0917) Ω cm^2 at 24 h, 0.4296(0.1056) Ω cm^2 at 48 h, 0.4225(0.0865) Ω cm^2 at 168 h, 0.4347 (0.0713) Ω cm^2 at 216h. These values represent an increase on the Rp at different time frames of 9.3 % at 24 h, 6.5 % at 48 h, 4.7 % at 168 h, 7.7% at 216h. On the other hand, there is a variable Rs over time, but after 216h, the increase only corresponds to an increase of 5.4 %.

One of the advantages displayed for the LSM cell infiltrated with via dip coating and coated with Mn and Co via ALD is the Cr-resistant as shown in the constant power density of when the cell is subject to SOFC operation under Cr volatile species (similar performance at 0h and after 240 h of operation). The constant LSM performance could be attributed to the protection/control of the formation of Cr insulating phases that block the active sites of the LSM air electrode. As the Bode plots in Figure 6c show, the main resistance changes are still attributed to the LSM air electrode. The LSM surface-modified cell presents changes in both the Ωic and polarization resistance, but the absolute degradation of the cell Rt is only 7.4 %(initial Rt=0.4710 Ω cm^2 ; 240 h Rt=0.506 Ω cm^2). Thus, the infiltrated solution with the simultaneous coating of Mn and Co could be used to prevent the degradation when the cell is subject to Cr contamination for SOFC operation at 750 °C.

Figure 8 and Table 6 show the evolution of the ohmic and polarization resistance for the LSM cell infiltrated with dip coating and coated with Mn and Co via ALD at different times of SOFC operation at 750 °C under Cr contamination.

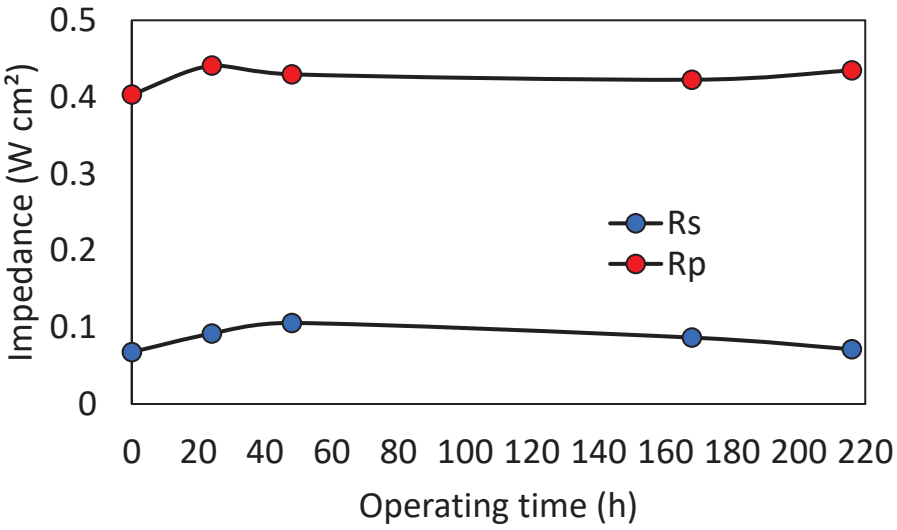

Figure 9: Evolution of ohmic (Rs) and polarization (Rp) resistance for the LSM infiltrated with via dip coating and coated with Mn and Co via ALD cell at different times of SOFC operation at 750 °C under Cr contamination.

Table 6: Numerical values obtained from impedance data of LSM infiltrated with dip coating and coated with Mn and Co via ALD cell showing the Rs and Rp at different times of 750 °C SOFC operations under Cr contamination.

	LSM coated 0 h	LSM coated 24 h	LSM coated 48 h	LSM coated 168 h	LSM coated 216 h
Rs (Ω cm²)	0.0676	0.0917	0.1056	0.0865	0.0713
Rt (Ω cm²)	0.4710	0.5327	0.5352	0.5091	0.5060
Rp (Ω cm²)	0.4033	0.4410	0.4296	0.4225	0.4347

Figure 8 shows the evolution of the terminal voltage when the LSM infiltrated with dip coating and coated with Mn and Co via ALD cell is operated at a constant current density of 0.3 A/cm^2 in SOFC mode under Cr contamination. The data from the terminal voltage plot shows the voltage remains constant for the duration of the long-term operation. For the SOFC operation under Cr volatile species, the voltage at different times is 0.929 V at 0h of SOFC operation, 0.914 V at 27 h, 0.915 V at 168 h, and 0.917 V at 240 h of SOFC operation. These values represent a change in voltage of 15 mV at 27 h (0.55 mV/h) or (0.05 %/h); 14mV at 168 h (0.08 mV/h) or (0.009 %/h); and 12 mV at 240 h (0.05 mV/h) or (0.005 %/h). There is an initial drop in voltage for the first ~27 h, but after the initial voltage drop, the cell performance is constant for the duration of the 240 h test. The overall V reduction for the SOFC operation with exposure to a Cr source when subject to a current density of 0.3 A/cm2 is 0.08 mV/h of operation or 0.005 %/h of operation. Including the

initial drop in voltage, the overall reduction corresponds to 1.3 % for the 240 h under Cr exposure in SOFC mode at 750 °C. Table 7 shows the values obtained from the terminal voltage data for the different SOFC parameters at different operation times.

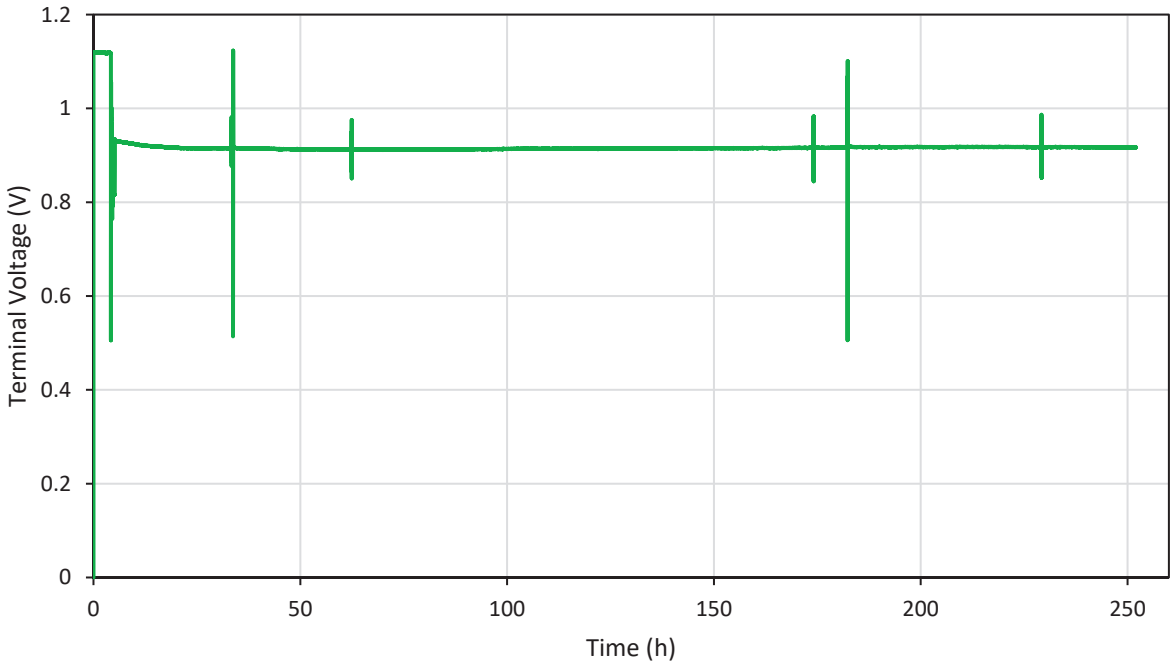

Figure 1 Evolution of terminal voltage when the LSM infiltrated with via dip coating and coated with Mn and Co via ALD cell is operated at constant current density of 0.3 A/cm2 in SOFC mode under Cr contamination. The peaks on graph correspond to the timeframe when impedance and power density analysis was taken.

Table 7: Numerical values obtained from terminal voltage data of LSM infiltrated with dip coating and coated with Mn and Co via ALD cell showing voltage drop when cell is operated at constant current of 0.3 A/cm^2 in SOFC mode with Cr contamination.

LSM inf & ALD Mn Co SOFC w/Cr source					
Time SOFC operation	Peak P(W/cm^2)	Peak ΔP (%)	I(A/cm^2)	V(V)	ΔV (mV) [% drop]
0 h	0.810	0	0.3	0.929	0 [0]
27 h	0.736	-9.1	0.3	0.914	15 [0.05]
168 h	0.809	-0.1	0.3	0.915	14 [0.00]
240 h	0.822	+1.5	0.3	0.917	12 [0.00]

5.4.4 Direct Comparison LSM baseline and surface modified LSM operated with Cr contamination

The electrochemical operation examinations at 750 °C showing the comparison of the sample with and without cathode surface modification in Figure 9. As previously discussed, the LSM baseline sample achieves a maximum initial peak power density of 0.862 W/cm^2 at 750 °C. On the other hand, the LSM sample achieves a maximum initial peak power density of 0.810 W/cm^2 at 750 °C, which is ~6 % lower than the LSM baseline. From Figure 8, the results show that the performance of the LSM baseline suffers a significant deterioration when the cell is being exposed to the Cr volatile species. The deterioration values of the LSM baseline are 0.605 W/cm^2 (-29.8 %) at 24 h, 0.450 W/cm^2 (47.8 %) at 50 h, 0.375 W/cm^2 (-56.5 %) at 74 h, and 0.307 W/cm^2 (-64.3 %) at 109 h. There is a big contrast when the LSM cell is infiltrated with and coated with Mn and Co via ALD. The deterioration of the cell is controlled with surface modification. The peak power densities for the modified LSM cell are 0.7361 W/cm^2 (-9.1 %) at 27 h, 0.8093 W/cm^2 (-0.1%) at 168 h, and 0.8225 W/cm^2 (+1.5%) at 240 h. The results indicate that the LSM cell infiltrated and coated with Mn and Co via ALD does not suffer degradation in performance under Cr contamination as compared to the almost 64 % degradation in only 109 h for the LSM baseline. There is some initial degradation at 27 h of operation that needs to be further investigated, but after 240 h of operation, the cell shows similar power density performance to the initial values. Furthermore, Table 8 shows the performance comparison of the baseline and the modified LSM cells at different V-I conditions.

Table 8: Numerical values obtained from the I−V−P curves at 750 °C for SOFC operation of baseline and surface modified LSM cell under Cr contamination.

LSM Infiltrated ALD Mn Co								
Performance	0 h		27 h		168 h		240 h	
V(V)	I (A/cm^2)	P (W/cm^2)	I (A/cm^2)	P (W/cm^2)	I (A/cm^2)	P (W/cm^2)	I (A/cm^2)	P (W/cm^2)
0.5	1.604	0.805	1.467	0.735	1.613	0.809	1.640	0.822
0.6	1.297	0.774	1.137	0.682	1.248	0.745	1.257	0.751
0.7	0.965	0.671	0.837	0.583	0.877	0.615	0.881	0.619
0.8	0.637	0.509	0.557	0.446	0.569	0.457	0.570	0.459
LSM Baseline								
Performance	0h		24 h		50 h		109 h	

V(V)	I(A/cm^2)	P(W/cm^2)	I(A/cm^2)	P(W/cm^2)	I(A/cm^2)	P(W/cm^2)	I(A/cm^2)	P(W/cm^2)
0.5	1.718	0.862	1.200	0.605	0.899	0.450	0.616	0.307
0.6	1.287	0.769	0.932	0.550	0.679	0.407	0.457	0.273
0.7	0.920	0.634	0.647	0.451	0.496	0.347	0.339	0.237
0.8	0.572	0.454	0.446	0.352	0.357	0.282	0.245	0.195

The ASR values for both the uncoated LSM cell and the surface-modified LSM cell are shown in Table 9. The LSM baseline cell shows 3.03 times increase after 109 h. On the other hand, the LSM surface-modified cell shows an initial ASR value of 0.3602 Ω cm^2 at 750 °C. The ASR value after SOFC operation under Cr exposure displays an initial 10.1 % increase at 27 h, but the subsequent 2.2 % reduction at 240 h for the LSM coated cell. The evolution of the ASR values shows that there is no significant degradation after 240 h of SOFC operation under Cr volatile species.

Table 9 Numerical values of ASR obtained from the I−V curves at 750 °C for SOFC operation of baseline and surface modified LSM cell under Cr contamination.

	Infiltrated & ALD Mn Co LSM				LSM Baseline			
	0 h	27 h	168 h	240 h	0 h	24 h	50 h	109 h
ASR (Ω cm^2)	0.3602	0.3967	0.3565	0.3523	0.3406	0.5053	0.6907	1.0322

The impedance plots are shown in Figure 6. The impedance of the LSM baseline cell shows minimum values of R_s=0.0610 Ωcm^2 and R_p=0.4241 Ωcm^2, at 750 °C, as shown from the Nyquist plot in Figure 10b. At the same time, the surface-modified LSM cell shows minimum initial values of R_s=0.0676 Ωcm^2 and R_p=0.4033 Ωcm^2, at 750 °C. Thus, the modified cell has ~10 % higher R_s values but 5 % lower R_p values compared to the initial performance of the LSM baseline. It is possible that the coating restricts the electrical connectivity, but there is a beneficial influence on the chemical reaction on the air electrode after the surface has been modified. When the LSM baseline is subject to a long-term test under Cr volatile species, the R_p values of the LSM baseline cell increase continuously with the duration of the test. The R_p values of the LSM baseline at different operation times are 0.5578 Ωcm^2 (31.5 %) at 24 h, 0.7065 Ωcm^2 (66.5 %) at 48 h, 0.8332 Ωcm^2 (96.4%) at 72 h, and 1.0101 Ωcm^2 (138.1%) at 100 h, where the value in parentheses shows the % increase compared to the initial performance. More notably, the R_p and R_s values for the surface modified LSM cell do not present any significant degradation after the continuous SOFC

operation under Cr volatile species. The changes for the modified LSM cell at different operation times for the R_p show values of 0.4410 Ωcm^2 (9.3 %) at 24 h, 0.4296 Ωcm^2 (6.5 %) at 48 h, 0.4225 Ωcm^2 (4.7 %) at 168 h, 0.4347 Ωcm^2 (7.7 %) at 216 h. On the other hand, there is a variable Rs over time, but after 216h, the increase only corresponds to an increase of 5.4 %. The deconvoluted spectra of the impedance data collected from the different cells operated at 750 °C and 0.3 A/ cm^2 are shown in Figure 10a. The peak of each element of the curve corresponds to a physical phenomenon that the cell experiences under operation, which represents the resistance arising from the physical processes of the cell. In the case of the LSM baseline with Cr exposure, the arc P2 seems to be increasing and shifting towards lower frequencies. This process contributing the largest portion of resistance will have the highest peaks and potentially hides the contribution of the P1 arc. The initial P2 arc at ~20Hz is attributed to the oxygen transport along with the surface/bulk in the air electrode. Therefore, when the LSM baseline is operated in SOFC mode with Cr exposure, the resistance of the phenomena (i.e., adsorption and charge transfer of oxygen in the cathode is restricted) increases which are shown in the high magnitude of arc P2. Comparing the LSM baseline with the deconvoluted data of the modified cell, it is noticeable that surface modification limits the degradation of the oxygen reduction reaction process in the electrode.

Figure 9 shows the evolution of the Ωic and polarization resistance for the baseline and the surface-modified LSM cell at different times of SOFC operation at 750 °C under Cr contamination. The continuous increase of the R_p value is observed for the LSM baseline for the duration of the SOFC operation. More notably, the R_p value remains nearly constant after an initial 9 % increase at 24 h.

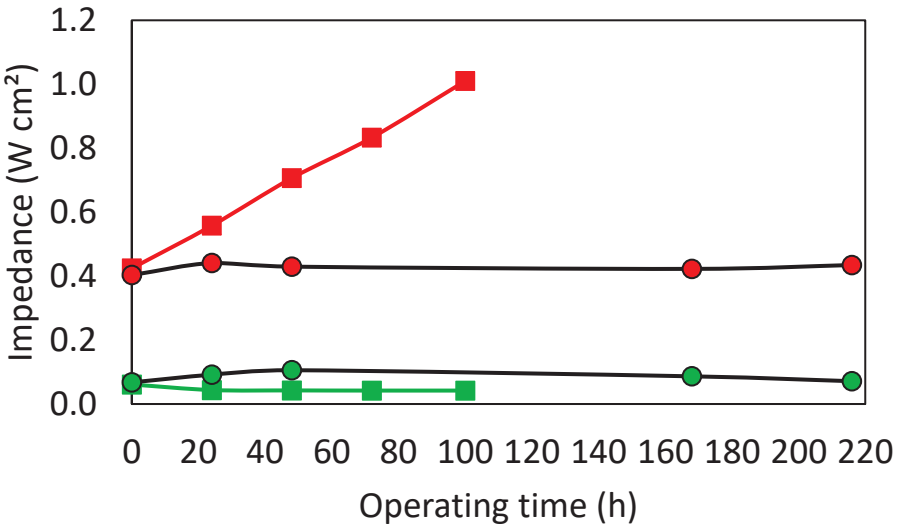

Figure 9: Evolution of Wic (Rs) and polarization (Rp) resistance for the baseline and modified LSM cells at different times of SOFC operation at 750 °C under Cr contamination.(Red, baseline, Green, surface modified. Square, polarization resistance, circle, ohmic resistance).

It can be observed from the results of the impedance data, and the I-V curves that the LSM cell infiltrated r via dip coating and coated with Mn and Co via ALD display superior resistance to Cr exposure, the power density of the cell show similar performance at 0h and after 240 h of operation and the impedance data show the improvement of physical properties compared to the LSM baseline. The physical origin of the Cr-resistant performance for the modified cell could be attributed to the protection/control of the formation of Cr insulating phases that block the active sites of the LSM air electrode. It can be inferred that the infiltrated with the simultaneous ALD coating of Mn and Co could be used to prevent the degradation when the LSM cell is subject to Cr contamination for SOFC operation at 750 °C.

Figure 10 shows the evolution of the terminal voltage comparing when the baseline and the surface-modified LSM cells are operated at a constant current density of 0.3 A/cm^2 in the SOFC mode under Cr contamination. The data plotted for the LSM baseline cell shows a big degradation in SOFC mode under Cr exposure. The voltage drop for different timeframes is shown in Table 10. The values represent a reduction in voltage of 28mV at 25 h (1.12 mV/h or 0.12 %/h); 76 mV at 50 h (1.52 mV/h or 0.16 %/h); 105 mV at 74 h (1.42 mV/h or 0.15 %/h); and 181 mV at 109 h (1.66 mV/h or 0.18 %/h). The drop in voltage corresponds to a 20 % reduction for the SOFC

operation with exposure to a Cr source when subject to a current density of 0.3 A/cm^2, and this is equivalent to 1.66 mV reduction for each hour of operation, which is equivalent to a 0.18 % reduction for each hour of operation. In contrast, the data plotted for the surface modified LSM cell shows the voltage remains constant for the duration of the long-term operation. There is an initial drop in voltage for the first ~27 h, but the cell performance is constant for the following 213 h duration of the test. The change in voltage values show 15mV at 27 h(0.55mV/h or 0.05%/h); 14mV at 168 h (0.08mV/h or 0.009%/h); and 12mV at 240 h (0.05 mV/h or 0.005 %/h). Including the initial drop in voltage, the overall reduction corresponds to 1.3 % (~5 %/Kh) for the 240 h long-term test under Cr exposure in SOFC mode at 750 °C.

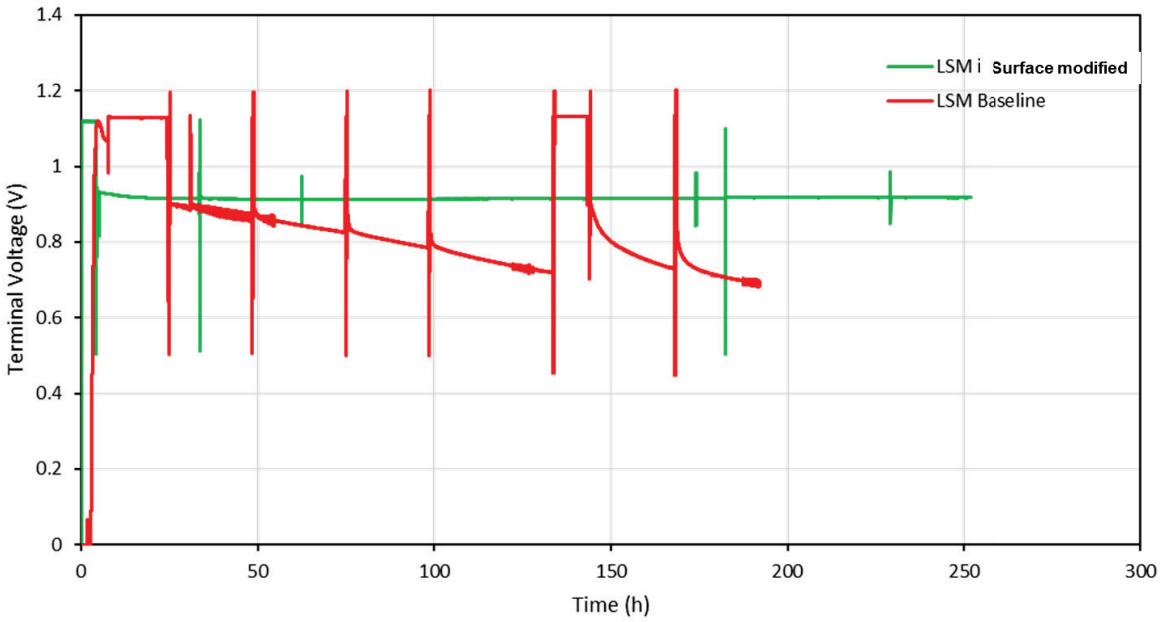

Figure 10 Evolution of terminal voltage when the LSM infiltrated with via dip coating and coated with Mn and Co via ALD cell is operated at a constant current density of 0.3 A/cm2 in SOFC mode under Cr contamination. The peaks on the graph corresponded to the timeframe when impedance and power density analysis was taken.

Table 10 Numerical values obtained from terminal voltage data of LSM infiltrated with via dip coating and coated with Mn and Co via ALD cell showing voltage drop when the cell is operated at a constant current of 0.3 A/cm2 in SOFC mode with Cr contamination.

	LSM Baseline SOFC w/Cr source				
Time SOFC operation	Peak P(W/cm^2)	Peak ΔP (%)	I (A/cm^2)	V(V)	ΔV (mV) [% drop]
0	0.862	0	0.3	0.900	0 [0]

25h	0.605	29.8	0.3	0.872	28 [3.0]
50 h	0.450	47.8	0.3	0.824	76 [8.4]
109 h	0.307	64.3	0.3	0.719	181 [20.1]

LSM inf & ALD Mn Co SOFC w/Cr source

Time SOFC operation	Peak $P(W/cm^2)$	Peak ΔP (%)	$I(A/cm^2)$	V(V)	ΔV (mV) [% drop]
0	0.810	0	0.3	0.929	0 [0]
27 h	0.736	-9.1	0.3	0.914	15 [0.05]
168 h	0.809	-0.1	0.3	0.915	14 [0.00]
240 h	0.822	+1.5	0.3	0.917	12 [0.00]

5.4.5 Improved Nanostructure Stability of Surface Modified LSM Cell operation with Cr contamination

Coating of the cell is necessary in order to mitigate the severe degradation of the LSM baseline cell after the long-term electrochemical operation under a Cr-rich environment. In the ideal approach, a fully conformal ALD coating layer on the internal surface of the air electrode should prevent Sr outward diffusion and prevent Cr inward diffusion, be highly active towards electrochemical reactions to limit performance degradation and be extraordinarily stable upon the electrochemical operation at elevated temperatures. To apply this approach, an LSM-CTG cell infiltrated via dip coating and coated with Mn and Co via ALD was subject to long-term operation under a Cr-rich environment, and the nanostructural examination was performed to evaluate the crystal evolution after the operation.

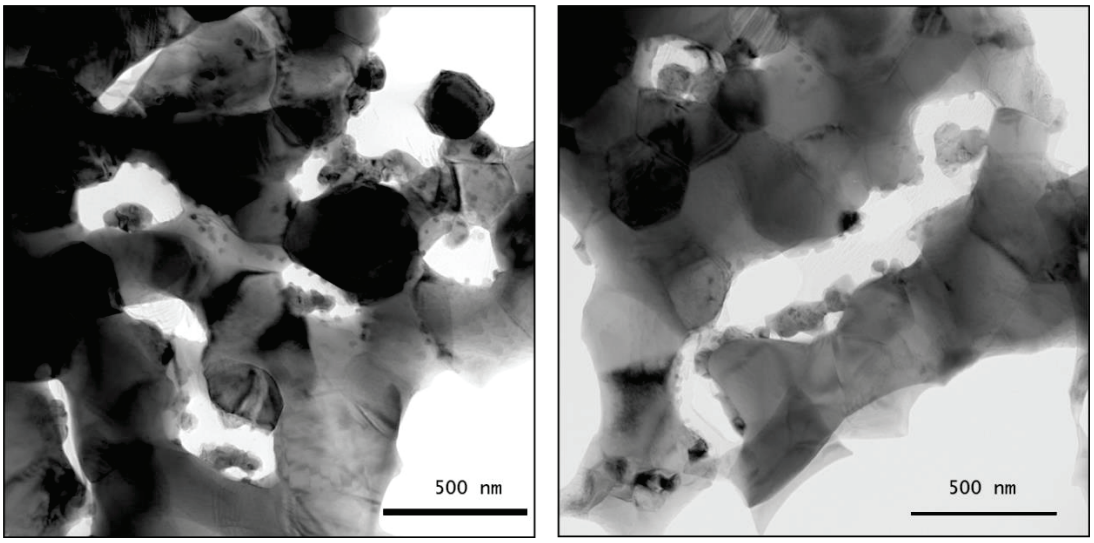

Figure 11 Surface modified LSM cathode after operation with Cr contamination for 250 h at 750 ^{o}C.

The nanostructure evolution of the cell infiltrated via dip coating and coated with Mn and Co via ALD is very different from that of the LSM baseline cell after long-term operation. Figure 11 shows the TEM examinations of the surface-modified cell after the long-term Cr-contamination exposure. There is a significant amount of Cr species deposit on the air electrode backbone, but the crystal structure seems to be stable even with the Cr-containing surface. The TPB regions do not seem to have deteriorated, and there are no pores in the LSM/SSZ interface. Additionally, the intragranular morphology of the LSM and SSZ crystals is stable after the long-term operation

5.5 Conclusion

For the commercial baseline cells, Cr contaminants on the LSM electrode severely impacted the electrochemical performance and nanostructure degradation of the entire cell. Those degradation include (1). Peak power density loss of 64% after 109 h operation. Dramatic increase in R_p (2). Cracking at LSM/SSZ interface, LSM grains. SSZ remains intact, but with (CrMn)Ox. By contrast, the electrode surface modification, including the ALD and ALD integrating with solution infiltration mitigate the electrode nanostructure degradation. The surface modification layer does not have to be fully conformal to prevent the original TPB region from cracking induced by Cr contamination. ALD coating (MnCo)Ox/Pt dramatically improves the Cr resistance, as follows (1). ALD coated cell is with power density is 280-380 % of the baseline cell depending on the ALD layer thickness. (2). For cell with a 20 nm thick ALD layer, there is a large performance enhancement (> 200 % power density) induced by ALD coating of Cr-tolerant $Mn_{0.8}Co_{0.2}O_x$. (3). For cell with 20 nm thick ALD layer, after 168 h at 750 ºC power density of ALD-coated cell is ~ 600 % of that baseline cell upon operation with Cr contamination for 109 h.

5.6 References

1 VOHS, J. M. & GORTE, R. J. 2009. High-Performance SOFC Cathodes Prepared by Infiltration. *Advanced Materials,* 21, 943-956.

2 CRACIUN, R., PARK, S., GORTE, R. J., VOHS, J. M., WANG, C. & WORRELL, W. L. 1999. A Novel Method for Preparing Anode Cermets for Solid Oxide Fuel Cells. *Journal of The Electrochemical Society,* 146, 4019-4022.

3 KIM, H., LU, C., WORRELL, W. L., VOHS, J. M. & GORTE, R. J. 2002. Cu-Ni Cermet Anodes for Direct Oxidation of Methane in Solid-Oxide Fuel Cells. *Journal of The Electrochemical Society,* 149, A247-A250.

4 GORTE, R. J., PARK, S., VOHS, J. M. & WANG, C. H. 2000. Anodes for direct oxidation of dry hydrocarbons in a solid-oxide fuel cell. *Advanced Materials,* 12, 1465-1469.

5 HE, H. P., HUANG, Y. Y., REGAL, J., BOARO, M., VOHS, J. M. & GORTE, R. J. 2004. Low-temperature fabrication of oxide composites for solid-oxide fuel cells. *Journal of the American Ceramic Society,* 87, 331-336.

6 LEE, S., MILLER, N., STARUCH, M., GERDES, K., JAIN, M. & MANIVANNAN, A. 2011. $Pr_{0.6}Sr_{0.4}CoO_{3\text{-delta}}$ electrocatalyst for solid oxide fuel cell cathode introduced via infiltration. *Electrochimica Acta,* 56, 9904-9909.

7 LEE, S., MILLER, N. & GERDES, K. 2012. Long-Term Stability of SOFC Composite Cathode Activated by Electrocatalyst Infiltration. *Journal of the Electrochemical Society,* 159, F301-F308.

8 Jiang, S. P. & Chen, X. Chromium deposition and poisoning of cathodes of solid oxide fuel cells – a review. *Int. J. Hydrog. Energy* 39, 505–531 (2014).

9 CHEN, Y., GERDES K. AND SONG X. 2016. Nanoionics and Nanocatalysts: Conformal Mesoporous Surface Scaffold for Cathode of Solid Oxide Fuel Cells, *Scientific Reports*, 32997, 2016.

10 Xiong, Y., Yamaji, K., Kishimoto, H., Brito, M. E., Horita, T. & Yokokawa, H. Deposition of Platinum Particles at LSM/ScSZ/Air Three-Phase Boundaries Using a Platinum Current Collector. *Electrochem. Solid State Lett.* 12, B31-B33 (2009).

11 Shin, S. M., Yoon, B. Y., Kim, J. H. & Bae, J. M. Performance improvement by metal deposition at the cathode active site in solid oxide fuel cells. *Int J Hydrogen Energ* 38, 8954-8964 (2013).

12 VAN HASSEL, B. A., BOUKAMP, B. A., BURGGRAAF, A. J. 1995. Electrode polarization at the Au, O_2(g)/Fe implanted yttria-stabilized zirconia interface *Solid State Ionics.* 51, 161.

13 KLEITZ, M., DESSEMOND, L., KLOIDT, T., STEIL, MC. DOKIYA, M. YAMAMOTO, O. TAGAWA, H. SINGHAL SC (Eds.), Proceedings of the Fourth International Symposium on Solid Oxide Fuel Cells, The Electrochemical Society, Inc, Pennington, NJ 1995, 527–536.

14 KLEITZ, M. 1995. Solid Oxide Fuel Cells IV. 44.

6 Cr Contamination on the Performance and Nanostructure of LSCF Cathodes

6.1 LSCF cathode and its intrinsic and extrinsic degradation

One critical issue in the development of reliable Solid Oxide Cells (SOC) technologies involves poor long-term durability over long-term as required for commercialization. Although SOC performance degradation can be caused by structural, thermal, chemical, and mechanical sources from various cell components, one major contributor to performance degradation comes from the oxygen electrode. Among these, surface segregation plays a crucial role in the chemical instability of oxide surfaces and the performance degradation of SOC electrodes and is a phenomenon generally associated with the redistribution and accumulation of specific cations at oxide surfaces due to a loss of symmetry at the surface relative to the bulk. A typical example involves A-site cation segregation, particularly Sr, which is frequently observed in Sr-containing perovskite-based electrodes such as LSM and LSCF annealed under oxidizing atmospheres and/or at SOC operating conditions and can occupy active surface sites and degrade electrochemical activities for oxygen reactions. Surface-segregated SrO is also highly mobile and can migrate across GDC barrier layers to form $SrZrO_3$ insulating layers on YSZ electrolytes. In addition, segregated SrO can interact with volatile impurities to form inert and nonreactive reaction products such as $SrCrO_4$, $SrSO_4$, and $SrCO_3$, causing the drastic poisoning of the electrocatalytic activities of oxygen electrodes. Based on all of this, the fundamental understanding of cation surface segregation is vital in the development of reliable and durable SOC technologies.

Numerous comprehensive reviews on cation segregation and its origin in perovskite oxide-based electrodes have been published on the segregation phenomenon, including influential factors, driving forces, reactivity with volatile impurities, mobility and interaction at the electrode/electrolyte interface, and the influence of electrochemical polarization on Sr-doped perovskite oxide electrode materials. However, there are discrepancies in the effects of influential factors on Sr segregation as reported by different groups. Sr segregation is critically influenced by a variety of factors. The differences in sample preparation processes, surface chemistry, surface

strains, surface morphology, atmospheres, impurities, and polarizations can have a critical effect on observed Sr surface segregation.

For the LSCF/SDC composite cathode, under SOFC operating conditions, the interaction between the LSCF and Fe-Cr alloy mainly results in the formation of $SrCrO_4$. [3,1] $SrCrO_4$ depositions on the electrode surface primarily hampered the gas transportation in the cathode. On the other hand, no $Co_{3-x}Cr_xO_4$ spinels have been observed on LSCF cathodes in contact with Fe-Cr alloy interconnect [2,3].

6.2 Experimental section

Commercially available, anode-supported solid oxide button cells fabricated by CTG (Salt Lake City, UT) were employed for all the experiments described in this paper. MSRI cells are composed of five layers as follows, starting from the anode: a ~700 μm thick Ni/YSZ cermet layer which supports the cell structure; a ~10 μm thick Ni/YSZ active layer; a ~10 μm thick YSZ electrolyte; a thin (2-3 μm), dense Sm_2O_3-doped CeO_2 (SDC) barrier layer, a ~10 μm thick LSCF/SDC active layer; and a 50 μm thick, pure LSCF current collecting layer. The cell active area (limited by the cathode) is 2 cm^2. The exposure area of the anode to fuel is about 3.5 cm^2. The ALD coatings were performed in a commercial GEMStar-8 ALD reactor from Arradiance Inc. No masking or specific treatment is applied on the NiO/YSZ anode before ALD processing. The thick and very dense NiO/YSZ anode prevents precursor penetration during the ALD processing, and the impact of ALD coating on the Ni/YSZ anode is negligible. No surface pretreatment or heat-treatment was applied before or after ALD coating either. The cell electrochemical operation was carried out directly after the ALD coating.

A set of experiments were carried out in a Cr-rich environment and a different set of samples were analyzed in a Cr-free environment to see the influence of Cr in the air electrodes of the cell. Inconel 600 mesh was used as Cr source to create a Cr-rich environment in the air electrode side. The active area of the cells is limited by the cathode, as such both the power density and current density are calculated considering this area even if the anode exposure to fuel is larger in area than

the active area of the cathode. In our test, the LSM/SSZ button cell as-fabricated by CTG was subject to operation on a single cell test station at 750 ºC under a Cr source for ~200 h. A multilayer-mesh stack was used as the inter-connect. The mesh stack includes 3 layers of Pt mesh and two layers of Inconel 600 mesh. The chemical composition of Inconel 600 used in this study is Al ~0.2, Co 0.03, Cr 16.05, Fe 8.6, Mn 0.45, Ni 73.7 Ti 0.21 and other 0.76 (all in wt %).

All cell tests were performed on a test stand. The platinum mesh was used for anode and cathode lead connections. The fuel and air stream flow rates were controlled separately using mass flow controllers. During the operation, a 400 mL/min air flow rate and a 400 mL/min fuel flow rate were used. Before any electrochemical measurements, both cells were current-treated for approximately ~15 h under a small current density of 0.1 A/cm^2 to ensure they were activated. After that, the samples were loaded at a constant current of 0.3 A/cm^2 for desired periods. The cell performance was examined using a TrueData-Load Modular Electronic DC Load, which guarantees voltage and current accuracies of 0.03 % FS of the range selected +/-0.05 % of the value. The cell impedance spectra were examined using a potentiostat/galvanostat (Solartron 1287A) equipped with a frequency response analyzer (Solartron 1260). Impedance measurements were carried out using a Solatron 1260 frequency response analyzer in a frequency range from 50 mHz to 100 KHz. The impedance spectra and resistance (ohmic resistance Rs and polarization resistance Rp) presented are those measured under a DC bias current of 0.3 A/cm^2. On a Nyquist plot, Rs is determined by the intercept at the higher frequency end, and Rp is determined by the distance between two intercepts.

After the electrochemical operation, the ALD coated cells were sectioned and subjected to nanostructural and crystallographic examination using high resolution (HR) Transmission Electron Microscopy (TEM). All the TEM examinations were conducted in the cathode active layer. TEM samples were prepared by mechanical polishing and ion milling in a liquid-nitrogen-cooled holder. Electron diffraction, diffraction contrast, and HRTEM imaging were performed using a JEM-2100 operated at 200 kV. Chemical analysis was carried out under TEM using energy dispersive X-ray Spectroscopy (EDS).

6.3 Baseline cell Electrochemical Performance Degradation

$La_{1-x}Sr_xCo_{1-y}Fe_yO_{3-\delta}$ (LSCF) based cathodes suffer from substantial degradation at their operational temperatures in the long term, especially associated with the Cr species evaporated from the metallic interconnect. In the cathode end, at high temperatures volatile Cr species such as CrO_3 and $Cr(OH)_2O_2$ are generated over the oxide scale in oxidizing atmospheres. Such volatile Cr species subsequently poison and react with the cathodes such as LSM and LSCF, causing a rapid degradation of the cell performance. Under SOFC operating conditions, the interaction between the LSCF and Fe-Cr alloy mainly results in the formation of $SrCrO_4$. This degradation occurs associated with Sr enrichment of the surface leading to suppressed oxygen surface exchange kinetics due to the insulating characteristics of SrO ($Sr(OH)_2$ and $SrCo_3$) species. These Sr species block the oxygen reduction reaction (ORR) active sites or passivate the entire surface of the cathode and the segregation is accompanied by a reduction in transition metal concentration. The underlying mechanism of this instability is not fully understood yet, but some hypotheses have been proposed such as kinetic de-mixing due to the greater mobility of Sr than other cations and surface charge effects due to electrostatic contributions. Two basic thermodynamic driving forces for Sr segregation have been identified: strain relaxation and smaller surface charge of SrO-terminated surfaces in comparison with LaO-terminated surfaces. The Sr surface segregation interacts with Sr and formed Sr and Cr enriched species such as $SrCrO_4$ that were deposited on the electrode surface primarily hampered the gas transportation in the cathode.

Depending on the electrode structure, the degradation of LSCF electrode degradation varies. Through this project, we have investigated the microstructure degradation of LSCF electrode upon Cr exposure, we have been working on the impact of the Cr poisoning on the commercial cells with different electrode structure. The LSCF/SDC button cell as-fabricated by CTG was subject to operation on a single cell test station at 750 C under a Cr source for 567 h. A multilayer-mesh stack was used as the inter-connect, and the chromium source.

Before operation, the cell was heated up to 750 ºC, reduced with 10 % H_2 and 33 % H_2 for ~ 6 h and then rest at open circuit voltage for overnight. After that, the cell was loaded with a current

density of 0.3 A/cm^2 and operated for 567 h as shown in Figure 2. The impedance data were taken periodically. During the operation, the cell had one interruption from 21 h to 110 h, in between which the current load was removed. Between 470 h and 520 h, the cell was still loaded with current. However, the terminal voltage was not collected because of the sensor lead problems.

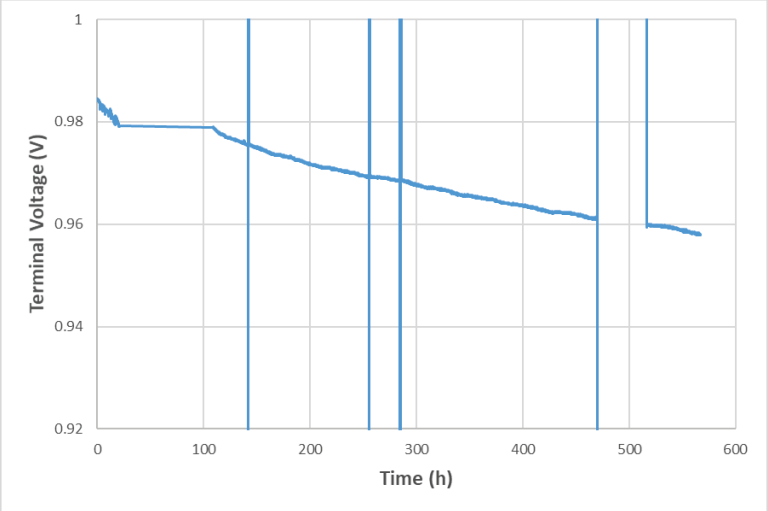

Figure 1 Terminal voltage as a function of time for the CTG LSCF/SDC cell operated at 0.3 A/cm^2 and 750 ^{o}C.

As shown in Figure 1, an immediate cell degradation was observed. In the entire operating period, the degradation rate is ~57 mV per 1000 h and the degradation is likely linear with the increase of the cell operation duration.

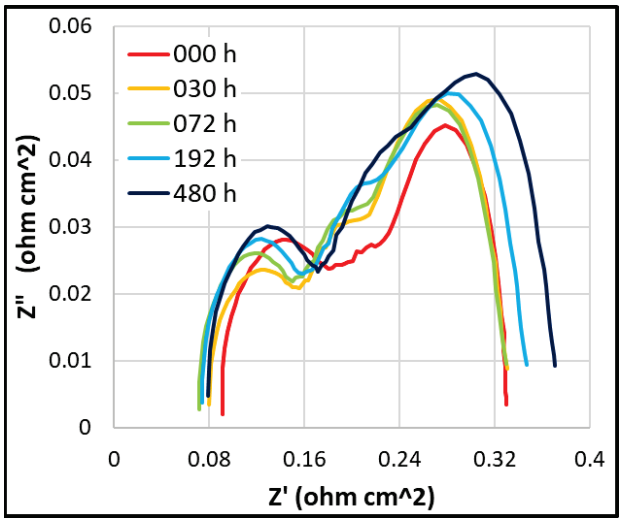

Figure 2 Nyquist plots of the cell as a function of operating time.

The Nyquist plots Figure 2 show that, upon the operation with Cr contamination, the series resistance R_s of the LSCF cell is 0.09 Ω cm^2 at 0 h and 0.08 Ω cm^2 at 30 h of operation. At 480 h,

R_s has little change of 0.08 Ω cm^2. On the other hand, the total resistance R_{total} increases, indicating polarization resistance increases a lot from 0.238 Ω cm^2 at 0 h up to 0.294 Ω cm^2 at 480 h. The cell shows significant degradation of its electrode activity upon operation.

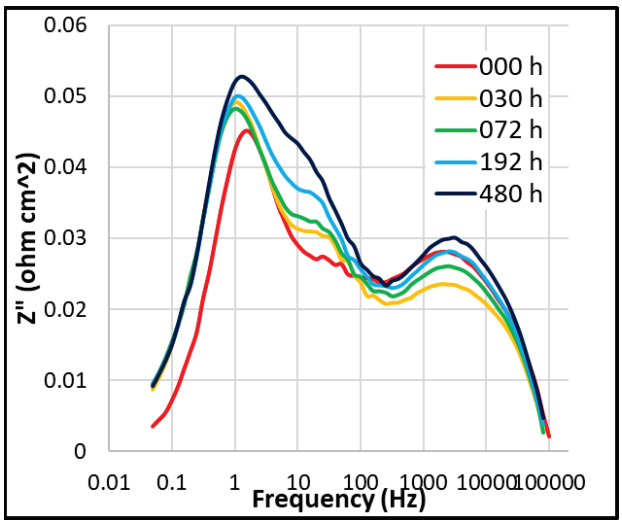

Figure 3 Bode plots of the cell as a function of operating time.

In Figure 3 of Bode plots, there is apparent increases of Z″ at f =0.5-1.5 Hz, f = 25 Hz and at f = 2500 Hz are seen. Further deconvolution (Figure 4) of the impedance data indicates the major changes of peaks are at 22 Hz, 125 Hz and 2000 Hz.

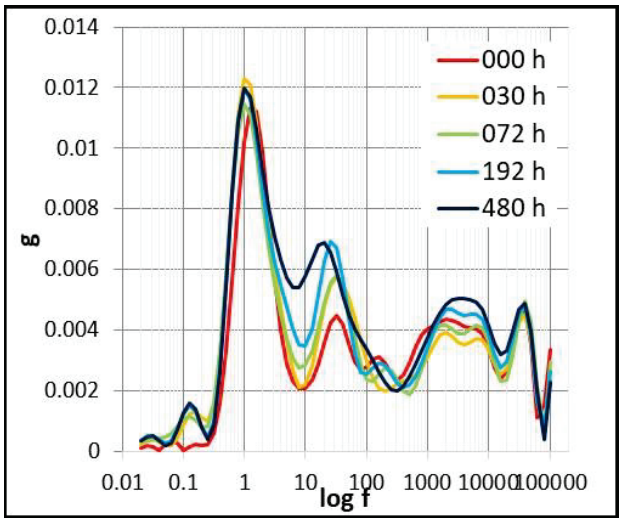

Figure 4 Deconvolution of impedance data.

The arcs at ~20-30 Hz could be possibly attributed oxygen reduction reaction activity at phase boundaries. The change of the arcs at 20-30 Hz for the cell is dominant, implying the cell lost its

ORR activity upon the operation in Cr contained environment. This could be attributed to the direct cover of Cr species at the LSCF surface or the reaction of Cr with backbone elements. While at frequencies around 2000 Hz, arcs were attributed to the charge transfer of hydrogen oxidation reaction and ionic transport at anode electrode. This is not corelated to the Cr contamination at the cathode side. The physical origin of the increase of the arcs at 2000 Hz needs to be further explored.

6.4 Baseline cell Nanostructure Degradation

6.4.1 LSCF/SDC cathode of commercial cells upon electrochemical operation without Cr contamination

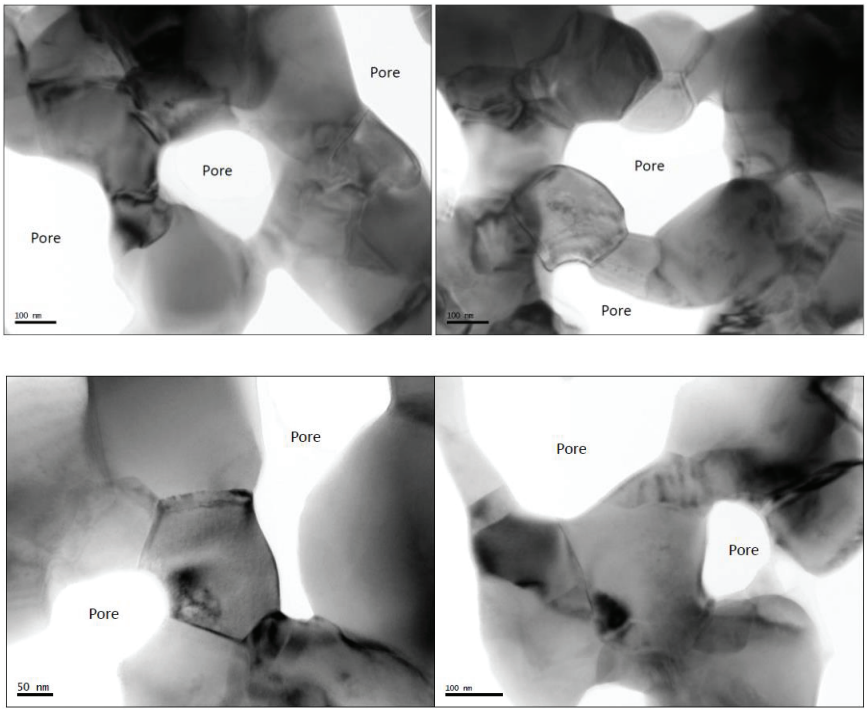

Figure 5 Typical TEM images of baseline LSCF/SDCAs received or operated for 3000 h at 750 oC without Cr contamination.

In the present study, the engineered cathode from the commercial cell is with a pore size of ~ 200 nm. Even after 3000 h of operation, the original pore presents the similar structure of the as-received cell and presents the same structure of the as-received cell. There is no detectable Sr surface segregation, and there is no formation of SrO_x on the internal surface of the backbone, as shown in Figure 5. The present study clearly indicated that under the commercial industry

operation relevant conditions, even after 3000 h of continuous electrochemical operation at 750 °C, there is no solid-state SrO oxide accumulated on the LSCF/SDC backbone internal surface.

6.4.2 Amorphous SrCrOx in the LSCF/SDC of upon electrochemical operation with Cr contamination

After the electrochemical operation, the same cell was subjected to the nanostructure and chemistry examination. For the LSCF baseline (cell without ALD coating), after the operation with Cr contamination source, some of the original pore regions is filled with the $SrCrO_x$.

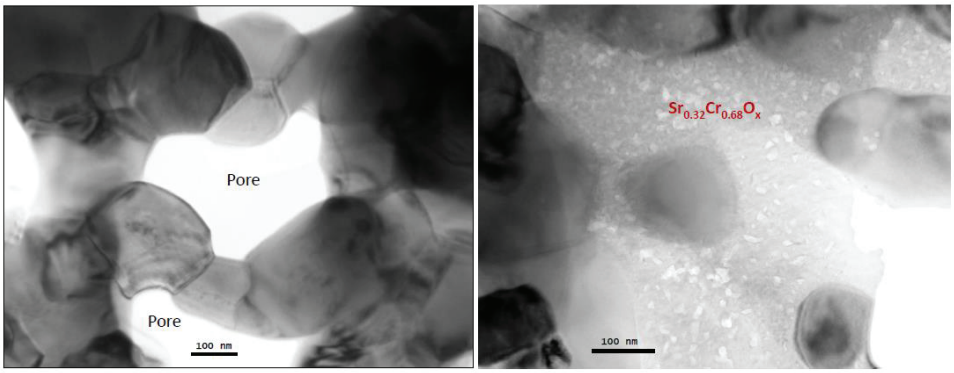

Figure 6 Direct comparison between the baseline cell operated without and with Cr contamination. (Left is Baseline LSCF/SDC, operation without Cr contamination, for 3000 h at 750 °C); (Right, for the LSCF baseline (cell without ALD coating), after the operation with Cr contamination source, some of the original pore regions is filled with the SrCrOx.

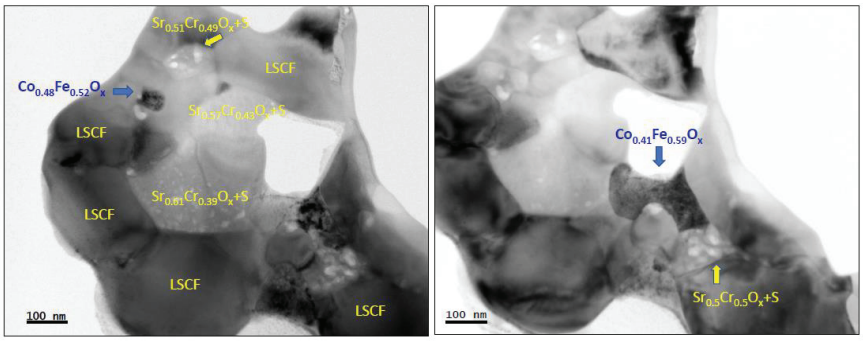

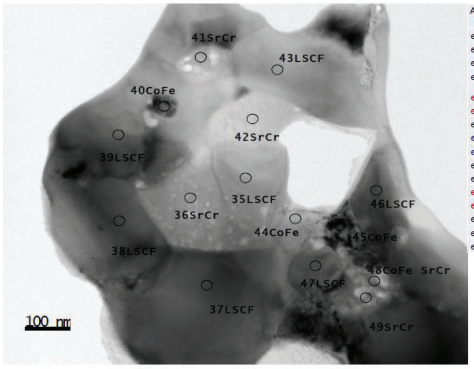

Atomic %	O	Cr	S	La	Sr	Co	Fe	Formula
eds-37	70.21			8.31	6.00	2.41	13.07	(La0.58Sr0.42)0.92(Co0.16Fe0.84)Ox
eds-38	74.52			7.68	5.14	1.97	10.69	(La0.60Sr0.40)1.01(Co0.16Fe0.84)Ox
eds-39	70.57			9.26	5.21	2.19	12.77	(La0.64Sr0.36)0.97(Co0.15Fe0.85)Ox
eds-40	74.52					12.18	13.31	Co0.48Fe0.52Ox
eds-41	75.46	12.07			12.47			Sr0.51Cr0.49Ox
eds-42	70.16	11.09	4.09		14.66			Sr0.57Cr0.43Ox+S
eds-43	75.77			7.29	5.47	2.07	9.39	(La0.57Sr0.43)1.11(Co0.18Fe0.82)Ox
eds-44	74.78					9.97	15.25	Co0.40Fe0.60Ox
eds-45	65.03					14.21	20.76	Co0.41Fe0.59Ox
eds-46	72.36			8.09	4.37	2.26	12.92	(La0.65Sr0.35)0.82(Co0.15Fe0.85)Ox
eds-47	73.17			9.49	4.82	1.48	11.05	(La0.66Sr0.34)1.14(Co0.12Fe0.88)Ox
eds-48	70.16	12.36			13.37	1.58	2.53	Sr0.52Cr0.48Ox+Co0.38Fe0.62Ox
eds-49	68.69	15.57			15.74			Sr0.5Cr0.50Ox
eds-50	71.57			8.37	4.50	2.38	13.18	(La0.65Sr0.35)0.83(Co0.15Fe0.85)Ox
eds-51	76.12			10.51	2.51	0.56	10.30	(La0.81Sr0.19)1.20(Co0.05Fe0.95)Ox
eds-52	69.81			7.85	6.13	2.70	13.50	(La0.56Sr0.44)0.86(Co0.17Fe0.83)Ox

For the LSCF baseline (cell without ALD coating), after the operation with Cr contamination source, some of the original pore region is filled with the Sr-Cr-Ox. There is Co-Fe-Oxide next to the Sr-Cr-Oxide phases.

Figure 7 Typical distribution of the SrCrOx enriched phases and the CoFeOx phases of the cell operated for 624 h with Cr contamination.

For the LSCF baseline (cell without ALD coating), after the operation with Cr contamination source, (1). some of the original pore regions are filled with the Sr-Cr-Ox. (2). There is Co-Fe-Oxide next to the Sr-Cr-Oxide phases. (3). For the LSCF-backbone, the LSCF chemistry remained the same as that original LSCF chemistry of $(La0.6Sr0.4)_{0.95}$ (Co0.2Fe0.8)Ox. (3). There is no apparent deviation of the stoichiometry changes due to the formation of the Sr-Cr oxide. (4). There is no interaction between the SDC backbone and the Sr and Cr.

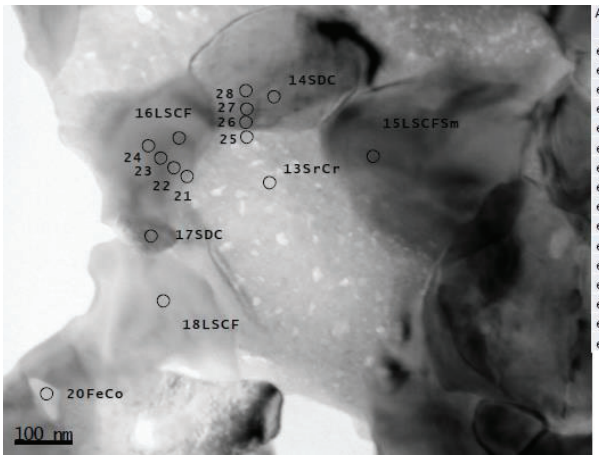

Atomic %	O	Cr	S	La	Sr	Co	Fe	Ce	Sm	Formula
eds-13	70.82	9.09	2.60		17.49					Sr0.66Cr0.34Ox+S
eds-14	77.74							19.92	2.35	Ce0.89Sm0.11Ox
eds-15	68.62			9.29	5.18	2.18	13.00		1.73	(La0.64Sr0.36)0.95(Co0.14Fe0.86)Ox
eds-16	75.85			7.04	4.78	1.98	10.35			(La0.60Sr0.40)0.96(Co0.16Fe0.84)Ox
eds-17	82.93							15.46	1.62	Ce0.91Sm0.09Ox
eds-18	78.44			7.53	4.00	0.49	9.53			(La0.65Sr0.35)1.15(Co0.05Fe0.95)Ox
eds-19	82.16					4.67	5.87	7.30		Co0.44Fe0.56Ox+Ce
eds-20	80.89					8.18	10.93			Co0.43Fe0.57Ox
eds-21	78.87			6.42	4.66	1.73	8.32			(La0.58Sr0.42)1.10(Co0.17Fe0.83)Ox
eds-22	77.81			6.72	3.88	2.03	9.56			(La0.63Sr0.37)0.91(Co0.18Fe0.82)Ox
eds-23	75.88			7.01	4.71	2.60	9.82			(La0.60Sr0.40)0.94(Co0.21Fe0.79)Ox
eds-24	73.99			7.84	5.98	2.57	9.63			(La0.57Sr0.43)1.13(Co0.21Fe0.79)Ox
eds-25	77.09	6.69	6.40		9.83					Sr0.60Cr0.40Ox+S
eds-26	79.12							19.31	1.57	Ce0.92Sm0.08Ox
eds-27	76.74							21.30	1.95	Ce0.92Sm0.08Ox
eds-28	74.94							21.92	3.14	Ce0.87Sm0.13Ox

Figure 8 Typical chemistry of the LSCF and SDC grains next to the SrCrOx that are accumulated in the original pore regions.

The above results from our project indicated that there is no observable solid state SrOx or the Sr surface segregation for the commercial cells operated for even 3000 h at 750 oC. However, the Cr sources, or the Cr vapor from the interconnect could play a key-role in the formation of the

solid-state SrCrOx that is accumulated in the original pore region of the LSCF/SDC backbone. It is worthwhile to point out that the SrCrOx phase is in amorphous state, and it is uniformly distributed in the original pore region similar to that of the accumulation of the liquid phase.

For the LSCF-backbone, the LSCF chemistry remained the same of that original LSCF chemistry of (La0.6Sr0.4)0.95 (Co0.2Fe0.8)Ox. There is no apparent deviation of the stoichiometry changes due to the formation of the Sr-Cr oxide. The SrCrOx is without La either.

This is very intriguing because the Sr in the SrCrOx is apparently coming from the backbone LSCF grains. The intact chemistry of the LSCF grains upon the formation of the SrCrOx (without La) imply that the La and Sr are probably departing the LSCF backbone at a similar rate. Because of the lack of the La or Sr solid phase in the baseline cells, the La and Sr may have vaporized during the electrochemical reactions at 750 ºC. Such vaporization of La and Sr species from the LSCF grains could be taking place on the cells without and with Cr contamination. For the cell without the Cr contamination, the Sr and La vapor would be taken away with the exhaust. However, when the cell is exposed to Cr contamination, the Cr vapor interacts with Sr or SrOx vapor and forms the solid-state amorphous. While at the 750 ºC where the cell operates, the formation of the La-Cr-Ox could be thermodynamically unfavorable.

Although the Sr surface segregation and the Cr contamination are well-known degradation cause for the SOFC community reported extensively during the past two decades, the results presented through this report are completely new to the research community. As such, the present study could have revealed two very important and unknown degradation mechanisms (1) Degradation of the LSCF/SDC baseline that is possibly incorporating the formation of the La Ox vapor and Sr-Ox vapors. By contrast, the formation of the solid-state SrOx is thermodynamically unfavorable (2). For the LSCF-SDC backbone, the Cr contaminations caused the formation of the SrCrOx amorphous phase due to the presence of SrOx vapor and the CrOx vapor. Such amorphous phase formation did not cause the major stoichiometry changes of the LSCF backbones due to the possible co-evaporation of the La and Sr species with a similar evaporation rate. Meanwhile, the formation of the SrCrOx and the evaporation of the La species results in the formation of residual

CoFeOx phases.

6.4.3 ALD coating and its impact on the performance and nanostructure of LSCF cathode

The PI of this project has also successfully identified the ALD layer chemistry and ALD processing conditions that are suitable for enhancing the performance and durability of the cell with LSCF/SDC backbone. In comparison with LSM/YSZ cathode, the LSCF cathode suffers from **low surface activity** for the oxygen reduction reaction[4,5,6] and **inadequate long-term durability**[7,8,9]. In order to enhance the surface activity of the LSCF/SDC cathode, the PI of this proposal chose the Pt as one of the choices for ALD layer. Prior to about year 1965, Pt was the only SOFC cathode material being considered extensively, until the transition metal oxide was investigated. LSCF based cells ideally need the conformal ALD layer to prevent Sr migration and Cr contamination. Several different kinds of ALD coating were developed through this project to prevent the Cr-contaminants attacking the LSCF backbone. This part of the data is currently under the processing of patent applications.

6.5 Conclusion

There are completely different nanostructure degradation mechanisms between LSM and LSCF cells induced by Cr contamination. LSCF based cells ideally need the conformal ALD layer to prevent Sr migration and Cr contamination. Without the Cr source, there is no apparent Sr surface segregation phase even for the baseline cell operated for 3000 h at 750 °C. With the Cr source, there is significant amorphous (SrCr)Ox phase accumulated in the original pore region. LSCF based cells ideally need the conformal ALD layer to prevent Sr migration and Cr contamination. Several different kinds of ALD coating were developed through this project to prevent the Cr-contaminants attacking the LSCF backbone. This part of the data is currently under the processing of patent applications.

6.6 References

1 Jiang, S. P.; Zhang, J. P.; Zheng, X. G., A comparative investigation of chromium deposition at air electrodes of solid oxide fuel cells. *J. Eur. Ceram. Soc.* 2002, *22* (3), 361-373.

2 Yokokawa H, Horita T, Sakai N, Yamaji K, Brito ME, Xiong YP, et al. Thermodynamic considerations on Cr poisoning in SOFC cathodes. Solid State Ionics 2006;177:3193e8

3 Schuler JA, Wuillemin Z, Wyser AH, Comminges C, Steiner NY, Van herle J. Cr-poisoning in (La,Sr)(Co,Fe)O3 cathodes after 10,000 h SOFC stack testing. J Power Sources 2012;211:177e83

4 OKAMOTO, H.; KAWAMURA, G.; KUDO, T. 1983. Electrochim. Acta, 28, 379.

5 HU, H.; LIU, M. 1997, J. Electrochem. Soc. 144, 3561.

6 SCHOULER, E., GIROUD, G., KLEITZ, M., 1973, J. Chim. Phys. 70, 1309.

7 VERKERK, M. J., BURGGRAAF, A. J. 1983. Oxygen Transfer on Substituted ZrO2, Bi2O3, and CeO2 Electrolytes with Platinum Electrodes I. Electrode Resistance by DC Polarization J. Electrochem. Soc. 130, 78.

8 LEWIS, R.; GOMER, R. 1968. Adsorption of oxygen on platinum, *Surf. Sci.* 12, 157.

9 MIZUSAKI, J., AMANO, K., YAMAUCHI, S., FUEKI, K. 1987, Electrode reaction at Pt, O2 (g)/stabilized zirconia interfaces. Part I: Theoretical consideration of reaction model, *Solid State Ionics* 22, 313.

7 Technical effectiveness & economic feasibility of ALD processing developed through this project

Solid oxide fuel cells offer high energy conversion efficiency, minimize emissions compared to combustion-based electrical power generation methods, and features excellent fuel flexibility. The cells are modular and scalable. SOFCs are with broad applicability including stationary power supply fueled by natural gas for residential use and portable power supplies in transportation applications. There are three primary segments of the market: stationary applications, transportation applications, and portable applications. The global solid oxide fuel cell market was estimated at approximately $175 million in 2017 and is expected to increase significantly to an estimated $1.4 billion by 2025. [1]

Growth in the market is expected to be driven by increased awareness about alternative energy applications, the global energy crisis. Most importantly, growth in the market is expected to be driven by the increased market competitiveness of SOFC technology in term of the cell power density, cell longevity, and cell/stack fabrication and maintenance cost.

7.1 State-of-the-art solution-based cathode infiltration and its technical barrier

One of the most reliable and efficient ways to further improve the performance of the SOFC cathodes is to modify the surface of the state-of-the-art cathodes to achieve enhancement in activity and stability. Electrode fabrication and modification by infiltration [2,3,4,5,6] of active components into a porous scaffold can achieve outstanding electrochemical performance. Over the past several years, solution-based infiltration processes have been developed for deposition of both discontinuous (discrete particle) and continuous (dense) coatings of catalysts into the state-of-the-art $La_{1-x}Sr_xMnO_3$ (LSM) and $La_xSr_{1-x}Co_yFe_{1-y}O_{3-\delta}$ (LSCF) cathodes, to enhance the surface electrocatalytic activity and stability [7,8]. Although solution-based infiltration of electrode/catalyst materials into a cathode scaffold may allow the use of a wide range of catalyst materials, several concerns need to be carefully considered. (1) Introducing the nanoscale electrocatalyst has been very challenging for the SOFCs because of the difficulty of penetration into the active layer, which is ~50 □m below the current collecting layer. In addition, sufficiently thick coatings must be

introduced to ensure low sheet resistance for efficient current collection, which is more important for larger cells or cell stacks. The need for large amounts of catalysts adds cost with respect to both fabrication with repeated infiltration steps and materials. (2) The degradation associated with the coarsening and sintering of nano-sized catalyst particles is potentially acute. Coarsening of the nanoparticles over the high temperature operation and loss of surface area and surface activity are problematic. (3) Due to the above, manufacturing scale-up of cathode infiltration is challenging, particularly in developing a low-cost process with simple processing requirement that remains versatile enough to accept many form features in materials.

7.2 Uniqueness of ALD and its technical challenge for SOFC applications

Uniqueness of ALD processing on SOFCs: ALD is a **chemical vapor deposition** technique that sequentially applied atomic monolayers to a substrate, typically alternating compounds to produce a locally balanced atomic distribution of the target material. [9] ALD is uniquely suitable for depositing uniform and conformal films on complex three-dimensional topographies with high aspect ratio. The indifference of ALD to substrate shape makes it particularly promising for applications to SOFCs, which presses porous active structure with complex three-dimensional topographies, and with electrode performance strictly depending on the surface properties. ALD processing is large batch and features easy scale-up and simplified handling precursors. Such capacity of ALD processing permits the simultaneous processing of hundreds of SOFCs.[10]

Technical challenges: Although ALD possesses significant promise as SOFC processing techniques, insufficient research has been completed to assure success in commercial applications. Recent work was reported for ALD coated symmetric cells [11,12] and some showed that the ALD coating symmetrical cells was detrimental to the cathode performance. [13, 14] Similar to conventional cathode infiltration, judicious selection of the ALD coating layer chemistry and crystal structure is critical achievement of the high cell performance. Several ALD coated material has been demonstrated detrimental for the cell performance, including SrO, CeO_2 and Al_2O_3.15

7.3 Uniqueness of ALD processing developed through this project

Determination efficacious materials and structures for application to commercial cells is

imperative to support commercial cell modifications using ALD. The results from this project have shown that significantly enhanced performance can be achieved by ALD infiltration of commercial cathodes. The ability to manipulate the surface chemistry of the mixed conductor and suppress its degradation related to the intrinsic Sr surface segregation is critical for the SOFCs. The present work demonstrates that, for the inherent functional SOFC with a mixed conducting composite cathode, the electrocatalytic nanoionics with high-density grain boundaries could be precisely introduced onto the cathode backbone. The conformal thin-film surface nanoionics can be controlled to have the single-layered, randomly orientated nanograins to maximize the contribution of surface grain boundaries and the interface strains to the conductivity and the electrocatalytic activities.

Overall, this project demonstrated a time efficient and scalable ALD coating to improve the power density of as-fabricated commercial cells. The conformal ALD layer completely shifted the ORR reduction pathways. It also serves as the effective barrier layer for backbone cations outward diffusion. Most importantly, the ALD coating turns the original perovskite surface that is vulnerable to cation segregation and degradation into an embedded strained interface phase with enormous conductivity. For the first time in the field of SOFC, our study demonstrates an effective approach for solving multiple problems for successfully suppressing the Sr surface segregation of mixed conductors, preventing Cr contamination, and simultaneously increasing the conductivity. The high-density surface and intergranular grain boundaries of the strained ALD layer provide an enormous surface area and interface area for facilitating multiple mass transport and catalytic reactions. It opens new research directions in terms of the fundamental design of the grain boundaries and strained critical interface for electrochemical reactions at elevated temperatures.

The ALD processing developed through this project features the following: (1) Simple and straightforward one step processing and time efficient. (2). Highly repeatable and controllable manufacturing processing. (3). Cost-effective. The surface architecture/scaffold possesses engineered nanostructure but features commonly used electrocatalyst materials. The developed surface layer possesses a minimum thickness of 10-20 nm and is solely designed to maximize the

TPB density. The fabrication methods offer precise structural control for maximum power density with minimum materials consumption. The ALD processing developed through this project thus bears immediate breakthrough on the SOFC technology since the applied ALD processing is scalable to both the single cells and SOFC stacks. Overall, the success of this project demonstrated the commercial scalability of the ALD processing with minimal impact to the cost structure of the cells and the stacks.

7.4 References cited

[1] Solid Oxide Fuel Cell (SOFC) Market Analysis by Application, by Region, and Segment Forecasts, 2018 –2025, Grand View Research, September 2017.

[2] VOHS, J. M. & GORTE, R. J. 2009. High-Performance SOFC Cathodes Prepared by Infiltration. Advanced Materials, 21, 943-956.

[3] CRACIUN, R., PARK, S., GORTE, R. J., VOHS, J. M., WANG, C. & WORRELL, W. L. 1999. A Novel Method for Preparing Anode Cermets for Solid Oxide Fuel Cells. Journal of The Electrochemical Society, 146, 4019-4022.

[4] KIM, H., LU, C., WORRELL, W. L., VOHS, J. M. & GORTE, R. J. 2002. Cu-Ni Cermet Anodes for Direct Oxidation of Methane in Solid-Oxide Fuel Cells. Journal of The Electrochemical Society, 149, A247-A250.

[5] GORTE, R. J., PARK, S., VOHS, J. M. & WANG, C. H. 2000. Anodes for direct oxidation of dry hydrocarbons in a solid-oxide fuel cell. Advanced Materials, 12, 1465-1469.

[6] HE, H. P., HUANG, Y. Y., REGAL, J., BOARO, M., VOHS, J. M. & GORTE, R. J. 2004. Low-temperature fabrication of oxide composites for solid-oxide fuel cells. Journal of the American Ceramic Society, 87, 331-336.

[7] LEE, S., MILLER, N., STARUCH, M., GERDES, K., JAIN, M. & MANIVANNAN, A. 2011. Pr0.6Sr0.4CoO3-delta electrocatalyst for solid oxide fuel cell cathode introduced via infiltration. Electrochimica Acta, 56, 9904-9909.

[8] LEE, S., MILLER, N. & GERDES, K. 2012. Long-Term Stability of SOFC Composite Cathode Activated by Electrocatalyst Infiltration. Journal of the Electrochemical Society, 159, F301-F308.

[9] MIIKKULAINEN, V., LESKELA, M., RITALA, M. & PUURUNEN, R. L. 2013. Crystallinity of inorganic films grown by atomic layer deposition: Overview and general trends. Journal of Applied Physics, 113. 021301.

[10] SKARP, J. I., SOININEN, P. J. & SOININEN, P. T. 1997. ALE-reactor for large area depositions. Applied Surface Science, 112, 251-254.

[11] GONG, Y., PATEL, R. L., LIANG, X., PALACIO, D., SONG, X., GOODENOUGH, J. B. & HUANG, K. 2013. Atomic Layer Deposition Functionalized Composite SOFC Cathode La0.6Sr0.4Fe0.8Co0.2O3-δ - Gd0.2Ce0.8O1.9: Enhanced Long-Term Stability. Chemistry of Materials, 25, 4224- 4231.

[12] GONG, Y., PALACIO, D., SONG, X., PATEL, R. L., LIANG, X., ZHAO, X., GOODENOUGH, J. B. & HUANG, K. 2013. Stabilizing Nanostructured Solid Oxide Fuel Cell Cathode with Atomic Layer

Deposition. Nano Letters, 13, 4340-4345.

[13] KÜNGAS, R., YU, A. S., LEVINE, J., VOHS, J. M. & GORTE, R. J. 2013. An Investigation of Oxygen Reduction Kinetics in LSF Electrodes. Journal of The Electrochemical Society, 160, F205-F211.

[14] YU, A. S., KÜNGAS, R., VOHS, J. M. & GORTE, R. J. 2013. Modification of SOFC Cathodes by Atomic Layer Deposition. Journal of The Electrochemical Society, 160, F1225-F1231.

8 Project conclusion

This project is aimed to develop a chromium (Cr) tolerant, highly active, and stable coating layer on the internal surfaces of the porous composite cathode from commercially available SOFCs. Such a coating layer was developed using the additive manufacturing process of Atomic Layer Deposition (ALD) and has been applied on the cathode consisting of either an electronic conductor of $La_xSr_{1-x}Mn_yO_{3-\delta}$ (LSM) or mixed ionic and electronic conducting $La_xSr_{1-x}Co_yFe_{1-y}O_{3-\delta}$ (LSCF).

The PI's work has demonstrated that the internal surface of cathode from the commercial cells, can be further tailored using ALD coating to dramatically enhance the cell performance. For instance, ALD layer consisting of heterostructured nano composite of nano-Pt and nano-$(Mn_{0.8}Co_{0.2})_3O_4$ oxide on the internal surface of porous LSM/YSZ cathode from SOFCs, has resulted in the large reduction of the cell polarizations resistance by up to 53%, and enormous increase of power density over 370%. For the cells with LSCF / Sm_2O_3 doped CeO_2 (SDC) cathode, the conformal layer of nano-composite consisting of superjacent CoO_x and subjacent minimum amount of Pt nano-grains has resulted in the power density enhancement by 126% for the large scale industry tubular cells at 750℃, and both the performance enhancement and nanostructure of the ALD layer are stable over ~ 2000 h continuous operation performed at industry test station. In the meanwhile, those ALD coating layer developed by PI's work is also inherently Cr-tolerant, and could act as physical barrier for preventing Cr diffusion into the cathode backbone, so as to mitigate the Cr poisoning effect on the cathode. In this project, the impact of Cr on the performance of those ALD coated commercial cells has been evaluated. Based on evolution of the cell performance, the ALD coating layer chemistry and ALD coating layer thickness has been optimized to maximize the overall Cr tolerance, cell power density and cell longevity.

Different ALD coatings have been applied onto the internal surface of LSM/YSZ and LSCF/SDC backbone respectively. The architecture/scaffold structures on the internal surface of different cathode, designed by this project, was catalogued and analyzed using High Resolution Transmission Electron Microscopy (HRTEM), and cell power/durability performance are assured

via comprehensive electrochemical performance testing in the industry operation relevant conditions. The impact of the electrochemical operation current density, the water humidity, the cell operation temperature, and cell operation duration on the Cr tolerance of ALD coated cells has been systematically investigated.

There are completely different nanostructure degradation mechanisms between LSM and LSCF cells induced by Cr contamination. For the LSCF/SDC baseline cell, With the Cr source, there is no apparent Sr surface segregation phase even for the baseline cell operated for 3000 h at 750 ºC. With the Cr source, there is significant amorphous (SrCr)Ox phase accumulated in the original pore region.

For the commercial baseline cells, Cr contaminants on the LSM electrode severely impacted the entire cell's electrochemical performance and nanostructure degradation. Those degradations include (1). Peak power density loss of 64 % after 109 h of operation. There is a dramatic increase in R_p .(2). They are cracking at LSM/SSZ interface, LSM grains. SSZ remains intact but with (CrMn)Ox deposition. By contrast, the ALD coating (MnCo)Ox/Pt dramatically improves the Cr resistance, as follows: (1). The ALD-coated cell with a power density is 280-380 % of the baseline cell, depending on the ALD layer thickness. (2). For a cell with a 20 nm thick ALD layer, there is a large performance enhancement (> 200 % power density) induced by an ALD coating of Cr-tolerant $Mn_{0.8}Co_{0.2}O_x$. (3). For a cell with a 20 nm thick ALD layer, after 168 h at 750 ºC power density of the ALD-coated cell is ~ 600% of that baseline cell upon operation with Cr contamination for 109 h.

The ALD coating on the internal surface of cathode developed by this project integrated multi-functions. Those multi-functions include (1). Dramatically improving the cell power density for the commercial cells; (2). Dramatically improving contamination resistance of the cathode, for being an excellent protection coating layer sealing off Cr contamination. (3). Dramatically increasing the cell longevity by potentially preventing the microstructure evolution and grain coarsening of the cathode.

Overall, this project will provide a simple solution to simultaneously enhancing power density and increasing the reliability, robustness, and endurance of commercial SOFCs, over the entire operating temperature range of 650-800 ºC. For the inherently functional SOFC, the ALD coating of LSM based cathode mitigates the Cr-contamination. Power density of ALD-coated cell is ~ 600% of that baseline cell upon operation with Cr contamination.

In addition to SOFCs, the novel on-demand design approach and creation of multifunctional heterogeneous architecture on the electrode surface presented in this work opens further research for their application in other types of fuel cells, batteries, and sensors for which electrochemical reactions on the surface are similarly critical.

9 Products developed

The results generated through this project have led to **three patent** applications as following:

(1) **Patent Application-1:** X. Song, Y. Chen, "Electrocatalytic Surface Nanoionics with Strained Interfaced and Colossal Conductivity For Enhancing Durability and Performance of SOFC".

- Date reported: January 15, 2021.
- U.S. Provisional Patent Application number, filed March, 2021.

(2). **Patent Application-2:** X. Song, Y. Chen, "ALD-Enabled Spontaneously Pinned Nano-Catalyst on the Internal Surface of Fuel Electrode of Solid Oxide Cells"

- Date reported: March 28, 2022.
- U.S. Provisional Patent Application number, filed June 6, 2022.

(3). **Patent Application-3:** Xueyan Song, Yun Chen, & Cesar-Octavio Romo-De-La-Cruz, "Atomic Layer Deposition- Enabled, Highly Efficient and Durable Solid Oxide Cells for Versatile Electricity Generation and Hydrogen Production",

- Date reported, April 14, 2022.
- U.S. Provisional Patent Application number, filed April 2022.

Upon the processing of the patent applications, the results from this project have also led to the publication of **several** journal papers that are currently at different stages of publication.